In-plane crushing behavior and energy absorption of a novel graded honeycomb from hierarchical architecture

Hu Liu[1], Ee Teng Zhang[1,2], Guangjian Wang[1,2], Bing Feng Ng[1,*]

[1]*School of Mechanical and Aerospace Engineering, Nanyang Technological University, 50 Nanyang Avenue, Singapore 639798, Singapore*

[2]*Singapore Centre for 3D Printing, School of Mechanical and Aerospace Engineering, Nanyang Technological University, 50 Nanyang Avenue, Singapore, 639798, Singapore*

Abstract

Nature's bio-organisms are typically hybrid structures composed of hierarchical and functionally graded micro-architectures, which are lightweight and of high mechanical performances. Inspired by nature, an innovative graded hierarchical honeycomb is proposed in this study to enhance its crashworthiness behaviors. The structure is created by replacing cell walls of regular honeycombs with triangular and hexagonal sub-structures and varying the hierarchical length ratio in each layer. The in-plane crushing performances of the graded hierarchical honeycombs are comprehensively analyzed and compared with their uniform hierarchical counterpart. The former exhibits a progressive deformation model under different impact velocities and three plateau stages can be observed under in-plane crushing loads through theoretical predictions. The triangular sub-structure presents better energy absorption than the hexagonal sub-structure, and its specific energy absorption is enhanced by up to 32.2% as compared to the uniform hierarchical honeycomb. The present study suggests that the combination of hierarchy and gradient is an effective strategy to improve the dynamic crushing behaviors of honeycombs, which can be further explored in protective devices to enhance their impact resistance.

Keywords: in-plane crushing; impact behavior; functionally graded; honeycomb; hierarchical; energy absorption.

* Corresponding author.

E-mail address: bingfeng@ntu.edu.sg (Bing Feng Ng).

Nomenclature of abbreviations

NGH	Negative gradient hierarchy
PGH	Positive gradient hierarchy
UH	Uniform hierarchy
NGH-Tri	Negative gradient hierarchy with triangular sub-structures
NGH-Hex	Negative gradient hierarchy with hexagonal sub-structures
PGH-Tri	Positive gradient hierarchy with triangular sub-structures
PGH-Hex	Positive gradient hierarchy with hexagonal sub-structures
UH-Tri	Uniform hierarchy with triangular sub-structures
PGH-Hex	Uniform hierarchy with hexagonal sub-structures
FE	Finite element
SEA	Specific energy absorption
SHPB	Split Hopkinson Pressure Bar

1. Introduction

Recent developments in the fields of aerospace, electronics, automotive, and naval industries have triggered an extraordinary demand for lightweight materials with superior mechanical properties. Promising candidates include various forms of honeycomb structures that can be designed to exhibit excellent characteristics in terms of specific stiffness, strength, impact resistance, and energy absorption. It is widely acknowledged that the key to achieving such outstanding mechanical behaviors lies in the structural topology. In this regard, various forms of hexagonal [1-3], Kagome [4], circular [5-7], and triangular [8, 9] honeycombs have been proposed and analyzed, in which the hexagonal structure is most commonly adopted for its outstanding mechanical properties [10] and wide existence in nature [11]. In this study, leveraging on the benefits of hexagonal structures and to further enhance their properties, the concepts of functionally graded and hierarchical architectures inspired from nature are introduced to the hexagonal honeycombs with triangular and hexagonal sub-structures.

Focusing on hexagonal honeycomb, theoretical and numerical studies revealed their excellent crashworthiness performances under in-plane [12-14] and out-of-plane [15, 16] impact loadings. In addition, the hexagonal honeycomb was also widely employed as the core material to enhance

the mechanical performance of lightweight sandwich structures [17-19]. To improve the in-plane and out-of-plane crushing characteristics of hexagonal honeycombs, the self-similar topology [20-23] and horseshoe cells [24] were widely developed by several authors. These studies all indicate that the hexagonal honeycomb is an effective structure to resist impact, and their dynamic behaviors can be captured effectively through numerical, theoretical, and experimental means. Honeycombs with other structural topologies have also been developed. For instance, the arc-shaped honeycomb was proposed to improve the energy absorption abilities and impact resistance behaviors of re-entrant honeycombs [25]. Similarly, the petal-shaped meso-structure was introduced into circular-celled honeycombs to enhance their energy absorption behaviors [26]. The Kirigami [27] and Origami [28] inspired configurations were also adopted to increase the in-plane crushing resistance and energy absorption capacity of traditional honeycomb.

Recently, the honeycombs made of shape-memory materials were also fabricated by using 4D printing technology to obtain the reversible energy absorbers [29-31]. Additionally, shape optimization [32] and topology optimization [33] methods were also employed to develop lightweight lattice structures with novel topologies of unit cell. However, all the above-mentioned design concepts are only limited to honeycombs with single-order cellular configurations, which have the disadvantage of lower in-plane stiffness that restricts their potential applications.

To increase the in-plane stiffness of lightweight honeycomb materials, many studies have sought inspiration from nature. One of the solutions is the concept of hierarchical configuration [34-37], and the other is the functionally graded property [38]. Taking the bone as an example shown in Fig. 1, its inner structure is assembled both gradually and hierarchically [39]. As observed, the inner structure under different length scales exhibits many hierarchies, such as the hierarchical structures of osteons and lamellae with their length scale varying from macroscopic to microscopic. Moreover, graded distribution is also found on the bone structure at different locations at the same length scale, and such phenomenon can be clearly observed for the structure transiting from the inner trabecular bone to the outer compact bone. Other bio-organisms such as bamboo [40, 41] also present functionally graded and hierarchical cellular distribution. Inspired by these bio-structures, the present work intends to design a novel honeycomb with a combination of functionally graded and hierarchical concepts to further enhance their crashworthiness behaviors.

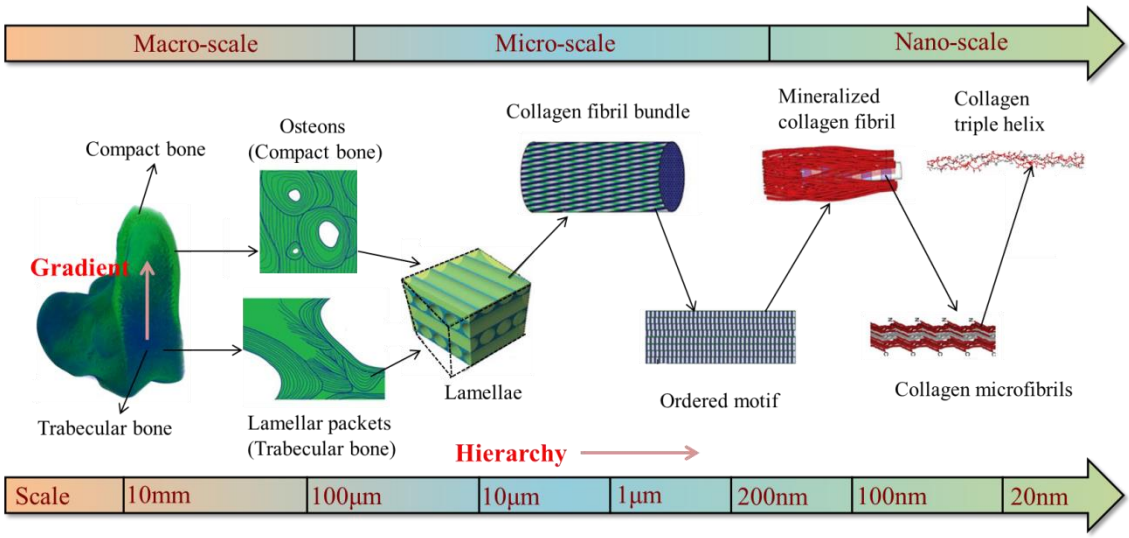

Fig. 1. Bone structure with graded hierarchical distribution [39]. As observed, the bone is composed of hierarchical and functionally graded microstructures.

The hierarchical hexagonal honeycomb is constructed by replacing the cell wall of the regular hexagonal honeycomb as a nested hierarchical structure. By using this method, hierarchical hexagonal honeycombs with triangular, Kagome, re-entrant, and chiral sub-structures were developed to enhance in-plane stiffnesses [42, 43]. Similarly, hierarchical honeycombs with hexagonal sub-architectures were proposed to improve in-plane elastic buckling behaviors [44]. In terms of in-plane and out-of-plane crashworthiness behaviors, hierarchical honeycombs possess higher energy absorption capacities as compared to traditional hexagonal honeycombs [45-49]. As a result, hierarchy was introduced to the design of lightweight metamaterials to enhance mechanical behaviors [50, 51]. All these studies demonstrate that the hierarchical honeycomb is able to combine the advantages of the regular honeycomb with the hierarchical cellular structures, resulting in significant enhancements to crashworthiness performances.

The concept of gradient is another bio-inspired strategy to further enhance the stiffness, strength, and toughness of honeycombs, which has been demonstrated through theoretical [2, 52], numerical [53-55], and experimental [56] means. The graded hexagonal honeycombs can be created by varying the thickness of each layer and have been shown to enhance overall crashworthiness performances [57, 58], and this graded design is also able to improve the in-plane crushing behaviors of re-entrant hexagonal honeycombs [59]. Meanwhile, this graded honeycomb was also adopted as core material to enhance the energy absorption of sandwich structures [60, 61]. Similarly, metamaterials with graded thickness in the crushing direction were also developed to improve their crashworthiness behaviors [62-64], which are achieved through multi-morphology

[65, 66] and topology optimization [67] approaches. Apart from varying the thickness of each layer, gradient can also be achieved by varying the unit cell configuration of honeycomb in each layer [68]. This design of graded self-similarity honeycomb structure has the ability to improve in-plane energy absorption characteristics [69]. The gradient distribution can also be achieved by introducing the materials with different stiffnesses into the structural design to fabricate a hybrid soft-hard lattice structure [70].

In essence, gradient and hierarchy designs can separately enhance the in-plane mechanical behaviors of honeycombs but their combined effect is still unknown. In this study, a series of novel honeycombs with graded hierarchical structures is proposed by replacing the cell wall of the regular hexagonal honeycombs with triangular and hexagonal sub-structures, and the gradient is achieved by varying the hierarchical length ratio in each layer. Their in-plane crushing performances are numerically and theoretically investigated and compared against traditional uniform hierarchical honeycombs. Additionally, the influences of gradient configuration and impact velocity on crashworthiness and energy absorption are discussed in detail. Intuitively, these newly designed honeycombs can take advantage of not only hierarchy but also functionally graded features to improve the dynamic crushing behaviors of honeycombs and offer insights to the design of multifunctional lightweight structures with enhanced impact performances.

The following sections are arranged as follows: The geometric description of the proposed graded hierarchical honeycombs and the adopted methodology are presented in Section 2. In Section 3, experimental results are presented for the validation of the FE simulations. Subsequently, the low-velocity impact response of graded hierarchical honeycombs is analyzed numerically and theoretically in Section 4. Next, the crushing performances of graded hierarchical honeycombs under different impact velocities are studied in Section 5. Finally, Section 6 concludes the main findings of the present study.

2. Graded hierarchical honeycombs

In this section, the structural description of graded hierarchical honeycombs, as well as their relative density distribution will be discussed. Subsequently, crashworthiness parameters that reflect the crushing behavior are explained in detail followed by the finite element (FE) model for the graded hierarchical honeycombs.

2.1. Geometric description

As depicted in Fig. 2, the hierarchical topology is constructed by substituting the cell wall of regular hexagonal honeycomb with a nested hierarchical sub-structure. Here, four types of graded hierarchical honeycombs are taken into account as shown in Fig. 3, in which two honeycombs are constructed with triangular sub-structures, and the other two consist of hexagonal sub-structures. Additionally, two uniform hierarchical honeycombs with triangular and hexagonal sub-structures are used for comparison study. The dimensions L, H, and b are, respectively, the overall horizontal length, vertical length, and out-of-plane depth of the uniform and graded hierarchical honeycombs. The graded hierarchical honeycomb is established by varying the number of sub-cell contained in different layers, and two layers with the same number of sub-cells form a gradient layer, e.g., Gradient layer 1 is composed of Layers 1 and 2 that contained the same sub-cell, as shown in Fig. 2. Similarly, Layers 3 & 4 form Gradient layer 2, Layers 5 & 6 form Gradient layer 3. The contained sub-cells in each gradient layer are varied across each gradient layer. For graded hierarchical honeycombs, increased strength is associated with a highly refined hierarchy, and lower strength is associated with a coarsely refined hierarchy. The graded hierarchical honeycomb with strong top and weak bottom is treated as negative gradient hierarchy (NGH), while that with weak top and strong bottom is named as positive gradient hierarchy (PGH). To show the graded hierarchical distribution, the configurations of a periodic cell for each layer for NGH honeycombs are shown in Fig. 2, and the interfaces between Layers 2 & 3, as well as Layers 4 & 5 are clearly illustrated in Fig. 3.

The topology of hierarchy can be captured by two geometric parameters. The first parameter is N, which stands for the number of contained sub-cell placed on the central axis (red dashed line shown in Fig. 2). The other geometric parameter is the hierarchical length ratio $r_i = l_i / l_0$, which represents the length ratio of each sub-cell to the unit cell. The subscript $i = 1, 2, 3, \ldots$ denotes the gradient layer number of the graded hierarchical honeycombs marked from the bottom. l_i represents the side length of the sub-cells in i-th gradient layer and l_0 is the length of the regular honeycomb. Here, the length l_0 and edge thickness h for every unit cell are set as constant for all graded hierarchical honeycombs.

The gradient can be represented by varying the hierarchical length ratio r_i in each gradient layer of the honeycomb, and the number of sub-cells N_i is also changed accordingly, and they satisfy

$$r_i N_i = 1, \tag{1}$$

in which N_i is the number of sub-cells in i-th gradient layer. Taking the NGH honeycomb with triangular sub-structures (NGH-Tri) as an example, the hierarchical length ratio and the number of sub-cells for Gradient layer 1 are set as $r_1 = 0.2$ and $N_1 = 5$. Additionally, the hierarchical length ratio and the number of sub-cells for other gradient layers are fixed as $r_2 = 0.1$ and $r_3 = 0.05$, corresponding to $N_2 = 10$ and $N_3 = 20$ for Gradient layers 2 and 3, respectively. Additionally, the geometric parameters for the NGH-Hex honeycomb are set as $r_1 = 0.1$, $r_2 = 0.05$ and $r_3 = 0.025$, corresponding to $N_1 = 10$, $N_2 = 20$ and $N_3 = 40$ for Gradient layers 1, 2 and 3, respectively. Moreover, the hierarchy configurations for PGH-Tri and PGH-Hex are distributed in the opposite direction to those of NGH-Tri and NGH-Hex, respectively.

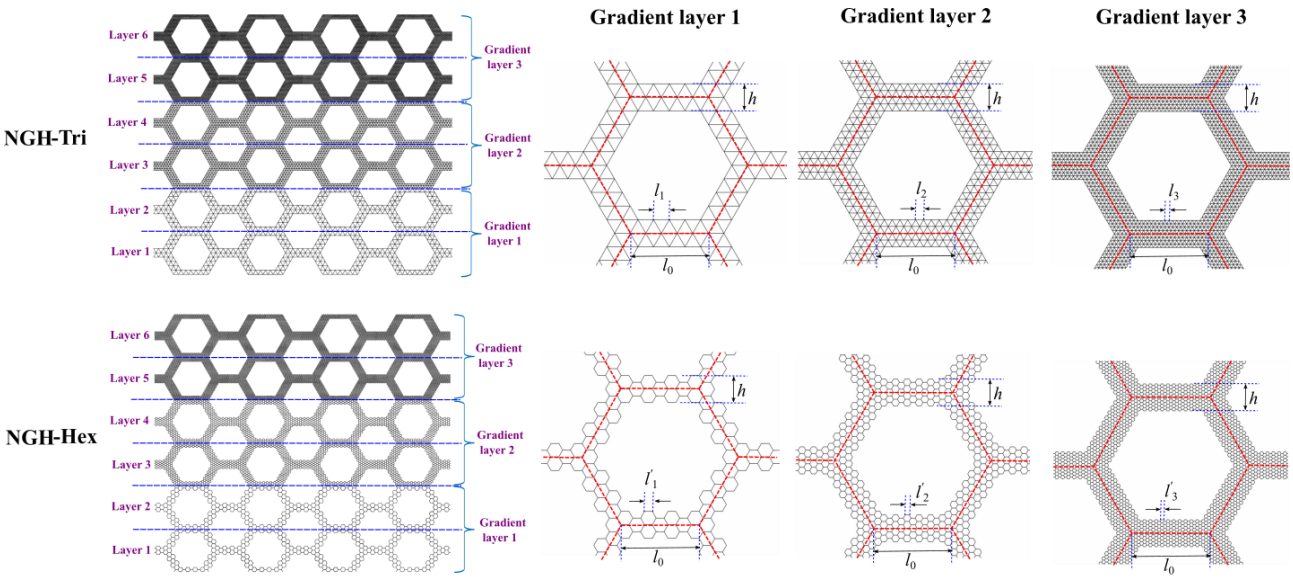

Fig. 2. Periodic cells for graded hierarchical honeycomb across different layers. Here, two layers with the same number of contained sub-cell form a gradient layer.

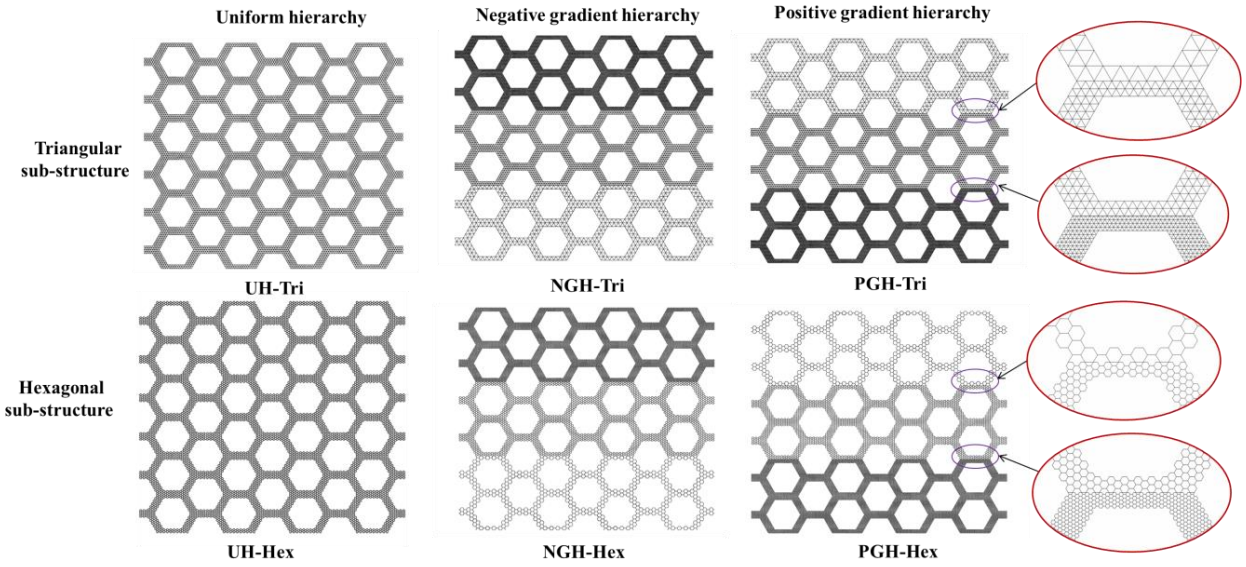

Fig. 3. Graded hierarchical honeycomb with triangular (-Tri) and hexagonal (-Hex) sub-structures. The NGH stands for the honeycomb with strong top and weak bottom, while the honeycomb with weak top and strong bottom is represented by PGH.

2.2. Relative density distribution

Similar to typical cellular materials, an important structural parameter used to determine the mass distribution of graded hierarchical honeycomb is the relative density that varies across different layers of the honeycomb. It can be approximated as the ratio of *i*-th gradient layered honeycomb's density ρ_i to the density ρ_m of parent material (the material from which the honeycomb is made). Additionally, relative density can also be calculated by the volume of honeycomb over the volume occupied by the unit cell, i.e.,

$$\bar{\rho}_i = \frac{\rho_i}{\rho_m} = \frac{V_i}{V_m}, \tag{2}$$

where V_i and V_m are the volume of *i*-th gradient layer and the volume occupied by the unit cell of the honeycomb, respectively. In this study, the volume occupied by the unit cell is the same for all four types of graded hierarchical honeycombs, which can be expressed as follows

$$V_m = \frac{3\sqrt{3}}{2} N_i^2 l_i^2 b, \tag{3}$$

where b is the out-of-plane depth of the honeycomb, N_i and l_i are the number and side length of the sub-cells in the *i*-th gradient layer of the graded hierarchical honeycomb, respectively.

The volume V_i is different for different graded hierarchical configurations. Taking NGH-Tri for example, the volume of honeycomb for different layers can be represented as

$$\begin{cases} V_1 = (21N_1 - 12) l_1 t_1 b \\ V_2 = (39N_2 - 42) l_2 t_2 b \\ V_3 = (75N_3 - 156) l_3 t_3 b \end{cases}, \tag{4}$$

in which t_i denotes the wall thickness of sub-cells. By substituting Eqs. (3) and (4) into Eq. (2), the relative densities for NGH-Tri honeycomb at different layers can be obtained

$$\begin{cases} \bar{\rho}_1 = \dfrac{2(7N_1 - 4)}{\sqrt{3}N_1^2} \dfrac{t_1}{l_1} \\ \bar{\rho}_2 = \dfrac{2(13N_2 - 14)}{\sqrt{3}N_2^2} \dfrac{t_2}{l_2} \\ \bar{\rho}_3 = \dfrac{2(25N_3 - 52)}{\sqrt{3}N_3^2} \dfrac{t_3}{l_3} \end{cases}. \tag{5}$$

Similarly, the relative densities for NGH-Hex honeycomb at different layers can be expressed as:

$$\begin{cases} \bar{\rho}'_1 = \dfrac{2(13N_1' - 10)}{3\sqrt{3}N_1'^2} \dfrac{t_1'}{l_1'} \\ \bar{\rho}'_2 = \dfrac{2(21N_2' + 30)}{3\sqrt{3}N_2'^2} \dfrac{t_2'}{l_2'} \\ \bar{\rho}'_3 = \dfrac{2(49N_3' - 250)}{3\sqrt{3}N_3'^2} \dfrac{t_3'}{l_3'} \end{cases}, \tag{6}$$

in which N_i' and l_i' are the number and the side length of the sub-cells in *i*-th gradient layer of NGH-Hex honeycomb, respectively.

Two types of graded hierarchical honeycombs are taken into account, in which the first type is obtained by fixing the cell wall thickness for all sub-structures at a constant value, i.e., graded hierarchical honeycomb with uniform thickness. The other type is varying the thickness in each gradient layer to make sure the total mass of the graded hierarchical honeycombs is the same as that of the uniform hierarchical honeycombs, i.e., graded hierarchical honeycomb with varying thickness. Employing this method, the cell wall thickness for each gradient layer can be obtained by setting the relative densities $\bar{\rho}_1$, $\bar{\rho}_2$ and $\bar{\rho}_3$ in Eqs. (5) equaling to that of uniform hierarchical honeycomb with triangular sub-structures, as well as by setting $\bar{\rho}'_1$, $\bar{\rho}'_2$ and $\bar{\rho}'_3$ in Eqs. (6) equaling to that of uniform hierarchical honeycomb with hexagonal sub-structures.

2.3. Crashworthiness criteria

To characterize the crashworthiness performance of graded hierarchical honeycombs under compression, several different crashworthiness criteria can be compared, as shown in Fig. 4. Firstly, the total energy absorption *EA* can be calculated once the typical nominal stress-strain

curve is obtained, i.e.,

$$EA = V_t \int_0^{\varepsilon_d} \sigma(\varepsilon) \mathrm{d}\varepsilon \,, \tag{7}$$

where V_t is the volume occupied by the whole graded hierarchical honeycombs. σ and ε are crushing stress and strain of graded hierarchical honeycombs under dynamic loads, respectively. ε_d is the densification strain.

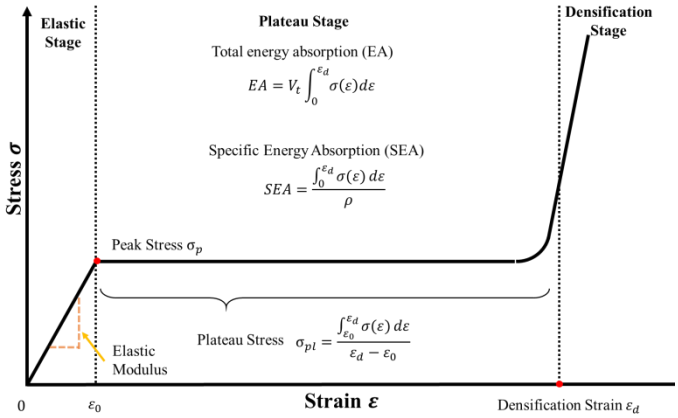

Fig. 4. Illustration of several different crashworthiness criteria for comparison study.

During the FE simulation, the crushing stress σ and strain ε can be obtained by

$$\sigma = \frac{F}{A_{\text{section}}} = \frac{F}{Lb}, \tag{8}$$

$$\varepsilon = \frac{\Delta H}{H}, \tag{9}$$

in which F stands for the reaction force in the impacting end, and ΔH is the moving distance of the impact end over the vertical direction.

Specific energy absorption (SEA) is an indicator that reflects the energy absorption capacity of graded hierarchical honeycombs, which can be defined by the ratio of total absorbed energy to the total mass of the specimen, i.e.,

$$SEA = \frac{EA}{M} = \frac{V_t \int_0^{\varepsilon_d} \sigma(\varepsilon) \mathrm{d}\varepsilon}{M}, \tag{10}$$

in which M denotes the total mass of the honeycomb.

The dynamic plateau stress (σ_p) over the plateau stage is another key parameter to assess the crashworthiness of honeycombs, which can be given as

$$\sigma_p = \frac{1}{\varepsilon_d - \varepsilon_0} \int_{\varepsilon_0}^{\varepsilon_d} \sigma(\varepsilon) \mathrm{d}\varepsilon \,, \tag{11}$$

in which ε_0 stands for the initial strain when the linear stress reaches its peak value. A higher value

of σ_p indicates that the honeycomb is more effective in energy absorption.

2.4. Numerical analysis

The numerical simulations related to the dynamic crushing behaviors of graded hierarchical honeycombs are performed using the nonlinear FE code ABAQUS/Explicit. As depicted in Fig. 5, the graded hierarchical honeycomb with 7 unit cells in *x*-direction and 6 unit cells in *y*-direction is taken into account, and its overall horizontal length L = 180mm, vertical length H = 155.9mm, and out-of-plane depth b = 2mm. It is assumed that the graded hierarchical honeycomb is made from aluminum alloy Al6063-T5, and the elastic, perfectly plastic material model is adopted to simulate its constitutive relation with its material properties presented in Table 1. The hardening behavior of this material can be captured by the Cowper Symonds power-law constitutive model [71]

$$\frac{\sigma_d}{\sigma_s} = 1 + \left(\frac{\dot{\varepsilon}}{\mathrm{D}} \right)^{1/\mathrm{n}}, \tag{12}$$

where σ_d and σ_s stand for the dynamic stress and quasi-static yield stress of the base material, respectively. $\dot{\varepsilon}$ is the von-Mises equivalent plastic strain rate used to represent the effect of strain-rate sensitivity of the material. D and n are material constants listed in Table 1.

Table 1 Material properties of aluminum alloy Al6063-T5 for graded hierarchical honeycombs.

Mass density ρ_s (kg/m^3)	Young's modulus E (GPa)	Poisson's ratio ν	yielding stress σ_0 (MPa) [12]	D (s^{-1}) [72]	n [72]
2700	69	0.3	76	128,800	4

It is known that the shell element is only suitable for structures with large length-to-thickness ratios. Here, the shell element is used to mesh the graded hierarchical honeycombs as the smallest length-to-thickness ratio for the cell walls is about 7.5:1. In fact, the reliability of shell elements on predicting the dynamic characteristics of honeycombs had been validated by several previous studies [2, 12, 69]. Herein, the element type for the cell wall of graded hierarchical honeycomb is treated as four-node, reduced-integration, shell elements (S4R), and five integration points along the thickness direction are adopted to ensure calculation precision.

The graded or uniform hierarchical honeycombs are fixed at the bottom and impacted by a rigid impactor axially from the top, with a constant velocity varying between 3 m/s to 60 m/s in

order to examine the influence of velocity on deformation modes and crashworthiness performances. As observed through experiments, the movement and rotational deformation for honeycombs mostly appear over the in-plane (i.e., in the *xy* plane), i.e., the deformation of the honeycomb satisfies the plane strain situation. Hence, the deformation along *z*-direction, the rotation across *x*- and *y*- directions for all nodes of the graded hierarchical honeycomb is constrained, while the deformation over the *x* and *y* directions, as well as the rotation across *z*-direction are all set as free to capture its in-plane crushing deformation. Additionally, to avoid possible penetration, an automatic self-surface contact is employed for all the cell wall surfaces of honeycombs during the plastic deformation, and the contact behavior between the graded hierarchical honeycomb and rigid impactor is simulated by the automatic note-to-surface contact criterion. The contact behaviors among different contact pairs can be captured by the definition of contact type as well as the friction coefficient. In this study, a penalty formulation with a friction coefficient of 0.2[26] is employed for the contact along tangential direction, while the contact along the normal direction is specified as 'hard contact'.

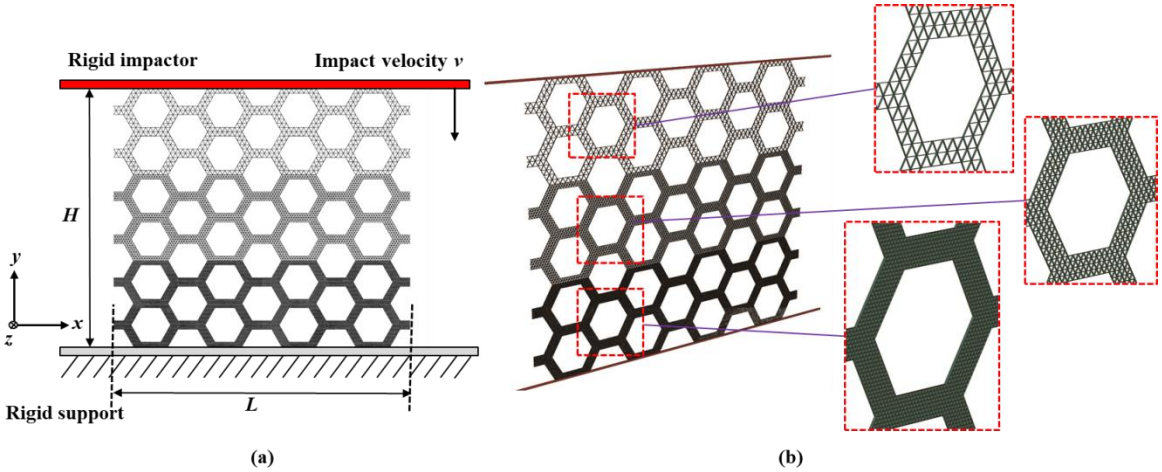

Fig. 5. FE model of graded hierarchical honeycomb under in-plane dynamic crushing: (a) front view; (b) isometric view.

To obtain a reasonable element size for the graded hierarchical honeycomb for the following simulation study, a mesh sensitivity analysis is performed firstly. The NGH-Tri honeycomb with thickness t = 0.05mm is taken into account, and four different element sizes including 0.8 mm, 0.4 mm, 0.3 mm, and 0.2 mm are employed for the convergence study. The crushing velocity is set as v = 15m/s in all these analyses. As observed from Fig. 6, the stress-strain curve and the SEA-strain curve converges as element size is refined. The deviations in the stress-strain curve and the

SEA-strain curve are large as the element size is changed from 0.8mm to 0.3mm, which becomes small when the element size is smaller than 0.3mm. To ensure computational accuracy, element size of 0.2mm is adopted. As a result, FE models with 447,660 and 417,912 elements are established for the graded hierarchical honeycomb with triangular and hexagonal sub-structures, respectively, as presented in Fig. 5.

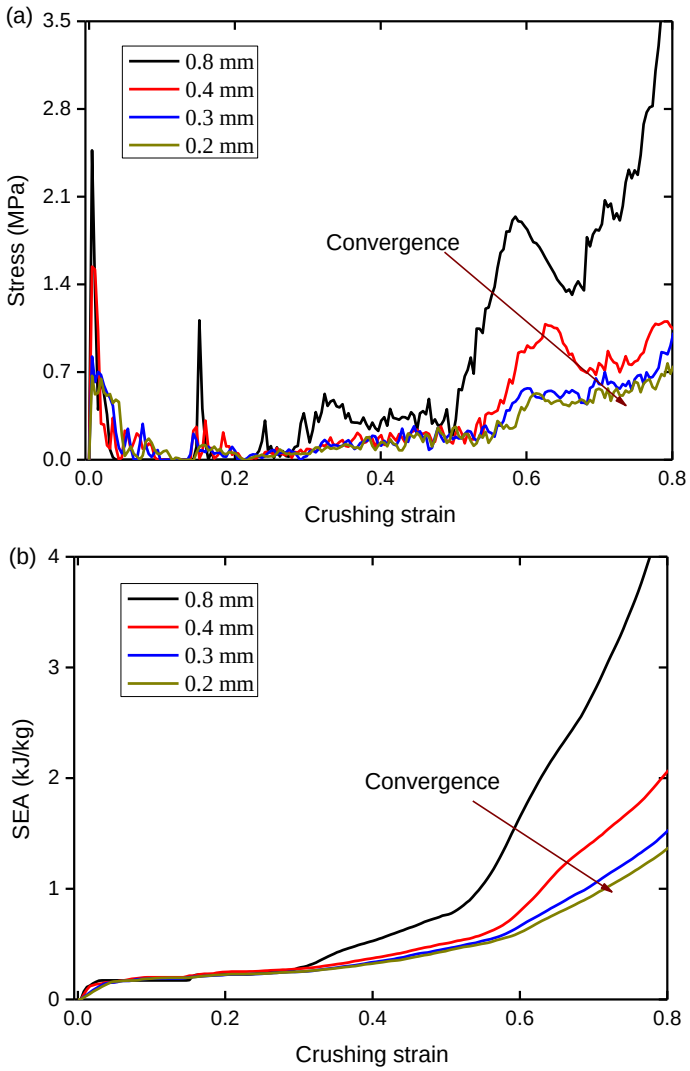

Fig. 6. (a) stress-strain and (b) SEA-strain curves for NGH-Tri honeycomb with different element sizes.

3. Validation of FE simulation method

In this section, some quasi-static compression experiments on the hierarchical honeycombs will be carried out firstly to give a validation of the proposed FE simulation method. The UH-Hex and UH-Tri honeycomb samples were fabricated through Stereolithography (SLA) 3D printing, which were then subjected to quasi-static compression tests to give a validation of the FE simulation method. A light-reactive thermoset material known as Grey-Pro resin was selected as the base material for production of samples using Formlabs Form3+. After printing, all samples

were washed and subsequently cured before compression experiment. Firstly, some dog-bone-shaped specimens were printed by using the same printing technology to obtain the material property of the base material, and dimension of the bone-shaped specimen is shown in Fig. 7(a), and the thickness of the specimen is 6 mm. The uniaxial tensile tests on the bone-shaped specimens were performed using the universal test machine with a tensile speed of 1 mm/min, and the specimens before and after tensile tests are exhibited in Fig. 7(b). The stress-strain curve of this base material is presented in Fig. 8. From this figure, Grey-Pro resin exhibits a typical elastic-plastic property with Young's modulus E = 1.1 ± 0.2GPa and yield stress σ_0 = 26.3 ± 0.3MPa.

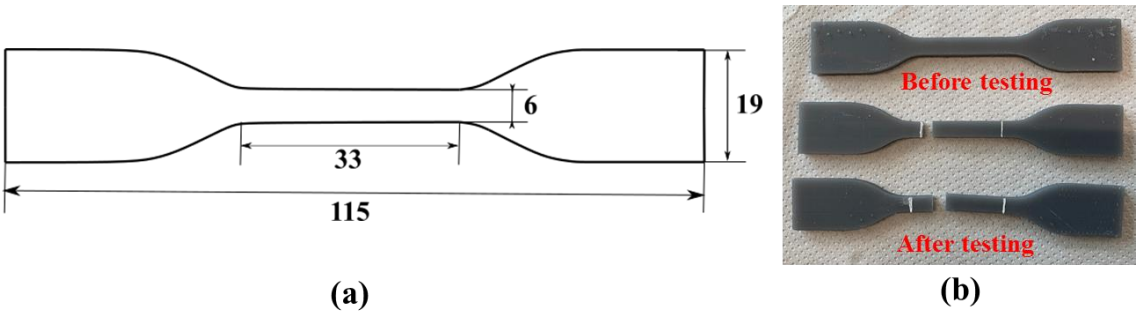

Fig. 7. Bone-shaped specimen for testing material properties: (a) Geometrical shape; (b) Specimens before and after uniaxial tensile tests.

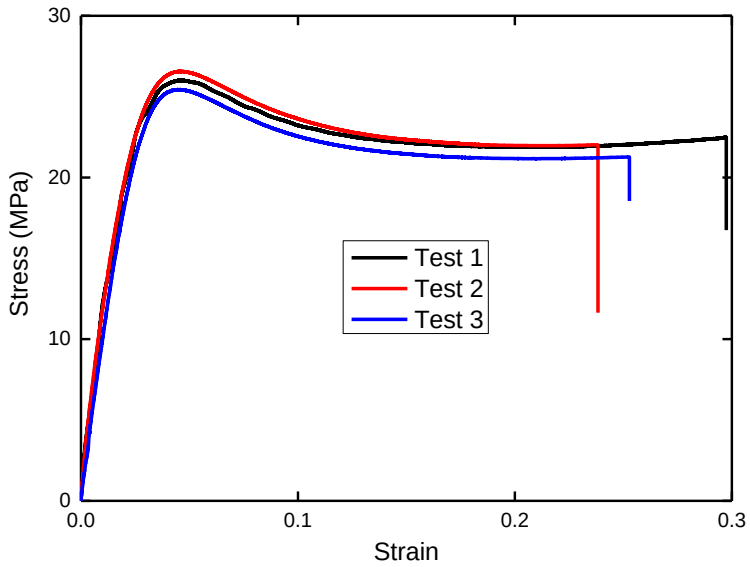

Fig. 8. Stress-strain curve of base material obtained by uniaxial tensile tests.

The UH-Hex and UH-Tri honeycomb samples with overall dimension 120 mm × 104 mm × 30 mm and thickness 0.3mm were taken into account, and the hierarchical length ratio for the UH-Hex and UH-Tri honeycombs is set as r = 0.1 and 0.2, respectively. The honeycomb samples were placed on a fixed plate and were crushed by a moving plate with a compression speed of

2mm/min ($0.02s^{-1}$). The FE model for the UH-Hex and UH-Tri honeycomb samples with the same geometrical parameters and same boundary condition is established, and the element size is set as 0.2mm by following the mesh sensitivity study in Section 2.4.

The deformation modes of UH-Hex and UH-Tri honeycombs predicted by the experiment and FE simulation are compared in Fig. 9 for different compression strains. One can find that the deformation pattern of UH-Hex and UH-Tri honeycombs from experiments are well captured by the FE simulations, verifying the latter's ability to analyze the crushing behaviors of hierarchical honeycombs. Moreover, the stress-strain curves of UH-Hex and UH-Tri honeycombs predicted by the FE simulations are compared to their experiments in Fig. 10. As observed, a slight deviation between the experiment and FE simulation can be found at the beginning and end of the compression test, which may be because the fracture of honeycomb samples are not taken into account in the simulations. Nevertheless, the plateau stresses and stress-strain curves from experiments can be captured well by the FE simulation and theoretical analysis (shown in Section 4.2), providing confidence that the present FE simulation method can provide sufficient accuracy in capturing the crushing mechanism of hierarchical honeycombs.

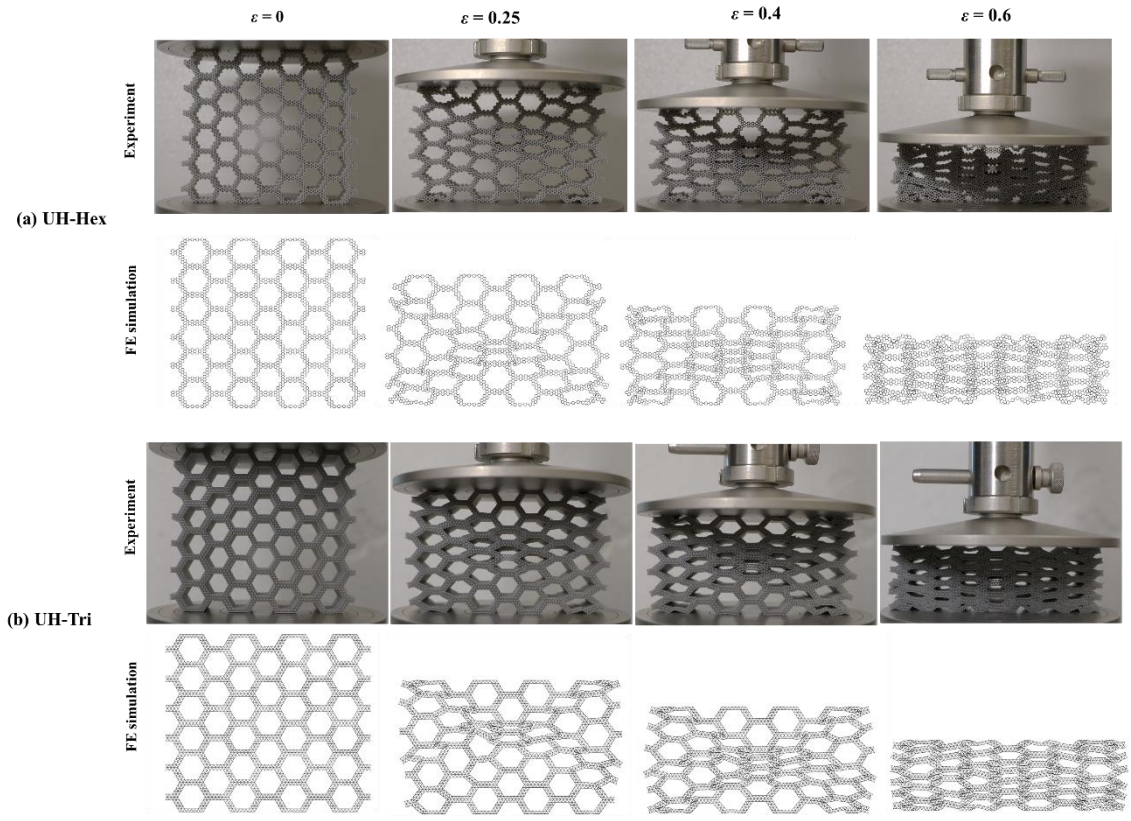

Fig. 9. Comparison between current experiment and FE simulation for deformation modes of (a) UH-Hex and (b) UH-Tri honeycombs under different compression strains, and a good agreement between current experiment and

FE simulation can be obtained.

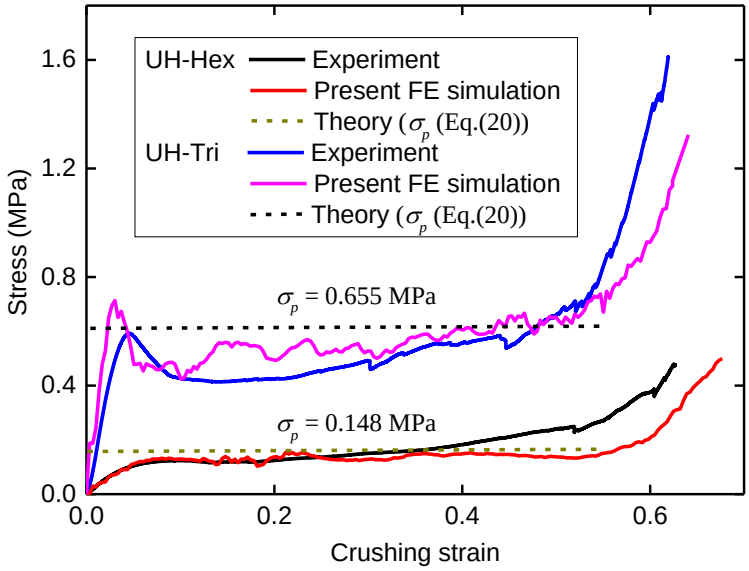

Fig. 10. Stress-strain curves of UH-Hex and UH-Tri honeycombs predicted by current experiment and FE simulation, indicating a good agreement between current experiment and FE simulation can be achieved.

4. Deformation pattern and collapse stress

To characterize the influence of sub-structure topology on the deformation pattern of the graded hierarchical honeycombs, their deformation modes and crushing stress-strain curve under low-velocity impact are summarized in Section 4.1. Subsequently, the theoretical methodology for predicting the plateau stress of the graded hierarchical honeycombs under compression is presented in Section 4.2, which is also compared to numerical results. Finally, the low-velocity impact performance of graded hierarchical honeycombs with varying thickness in different gradient layers is analyzed in Section 4.3 to give a comparison with the performance of honeycombs with uniform thickness presented in Section 4.1. In the following studies, to eliminate the influence of different total mass among different models, the comparative crushing stress is adopted by normalizing the crushing stress with their relative densities. Additionally, SEA is another normalized indicator through the total absorbed energy divided by the total mass of the honeycomb.

4.1. Low-velocity impact performance

The deformation modes for graded hierarchical honeycombs with hexagonal and triangular sub-structures under different crushing strains are presented in Figs. 11 and 12, respectively. Here, the impact velocity is set as v = 3m/s to represent low-velocity impact cases, and their thicknesses are set as t = 0.05mm. As observed, the “X” shear band is presented in the uniform hierarchical

honeycombs for both hexagonal and triangular sub-structural topologies. For the honeycombs with graded hierarchical distributions, the deformation first appears in the weak end, i.e., the top layer of PGH honeycomb or the bottom layer of NGH honeycomb. The deformation then progresses gradually towards the strongest layer of the graded hierarchical honeycombs, i.e., a progressive deformation pattern occurs. Moreover, this deformation pattern is related to the gradient distribution and is independent of the topology of sub-structures. The "I+V" deformation mode can be observed in each gradient layer. The hierarchical honeycombs are densified much earlier for the uniform configuration than those with graded hierarchical configurations, leading to a slightly larger densification strain for the graded hierarchical honeycombs.

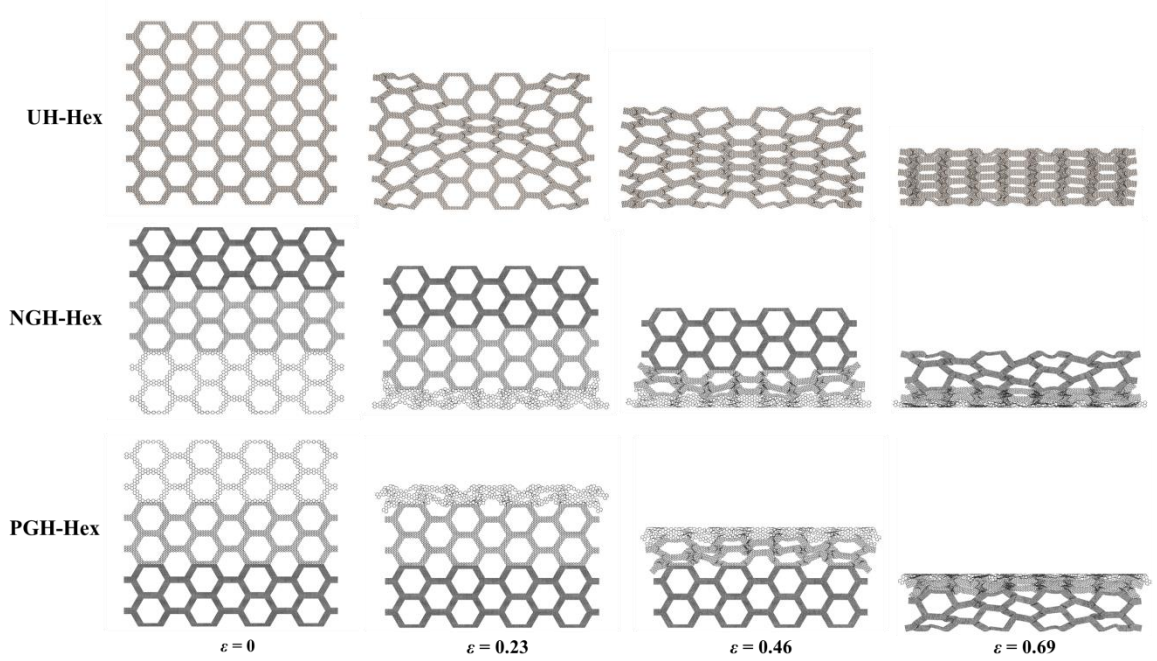

Fig. 11. Deformation pattern for graded hierarchical honeycombs with hexagonal sub-structures under low impact velocity v = 3m/s. The "X" shear band appears in UH-Hex honeycomb, while the "I+V" deformation appears first in the weak end and progresses gradually towards the strongest layer for NGH-Hex and PGH-Hex honeycombs.

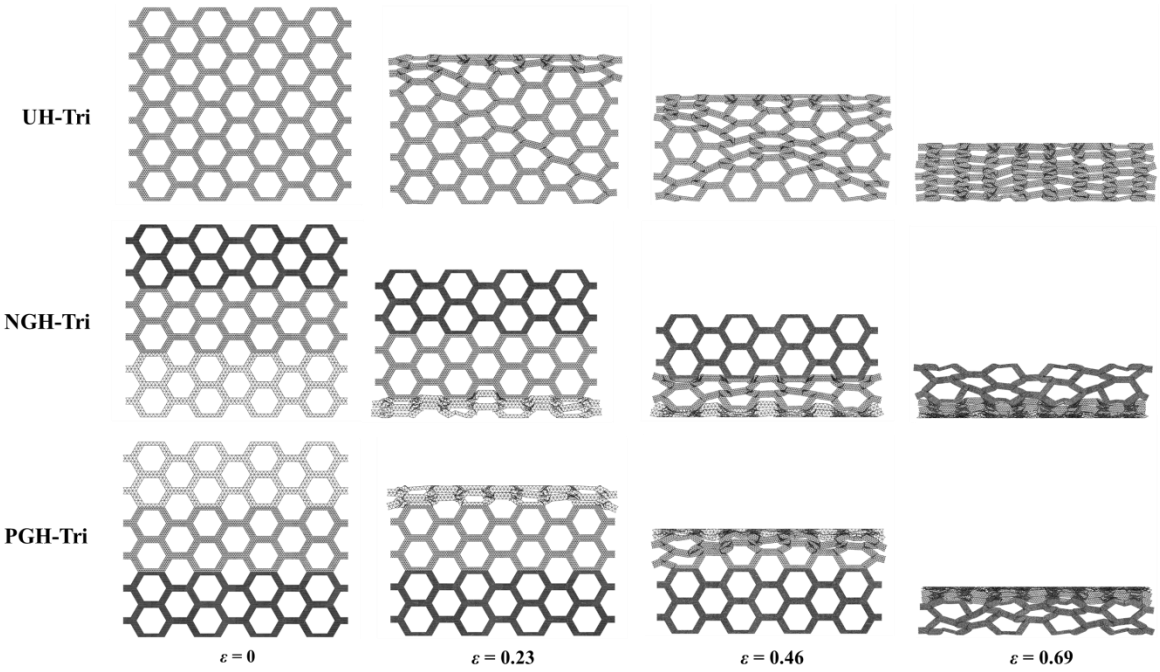

Fig. 12. Deformation pattern for graded hierarchical honeycombs with triangular sub-structures under low impact velocity v = 3m/s. The "X" shear band appears in UH-Tri honeycomb, while the "I+V" deformation appears first in the weak end and progresses gradually towards the strongest layer for NGH-Tri and PGH-Tri honeycombs.

The crushing stress-strain relations of graded hierarchical honeycombs with hexagonal and triangular sub-structures are depicted in Fig. 13 for the low-velocity impact conditions. Clearly, seven stages can be identified for the crushing response of graded hierarchical honeycombs under the low-velocity impact, and this mechanism is similar for both the hexagonal and triangular sub-structures. Stage I refers to the initial linear elastic response, which exhibits an approximately linear increase in stress over the strain and it ends as the initial yield stress is achieved. Subsequently, the first plateau region (Stage II) appears due to the crushing of the weakest layers of NGH and PGH honeycombs (shown in Figs. 11 and 12). In this stage, the crushing stress is stabilized by increasing the strain, which leads to large energy absorbed during this stage.

Stages IV and VI are the second and third plateau regions that correspond to the crushing deformation of the medium and strongest layers of the graded hierarchical honeycombs shown in Figs. 11 and 12. Stages III and V are two transitional stages that connect the two continuous plateau regions. During these stages, the crushing stress is increased from the previous plateau to the next one as the strain enhances. Stage VII stands for the final densification stage, in which most of the graded hierarchical honeycombs are densified, and the energy absorption efficiency will decrease by further deformation. On the other hand, the uniform hierarchical honeycomb only

exhibits a single plateau region during the crushing process. Additionally, the normalized stress for the graded hierarchical honeycomb with triangular sub-structures is almost 2.5 times larger than that for graded hierarchical honeycomb with hexagonal sub-structures.

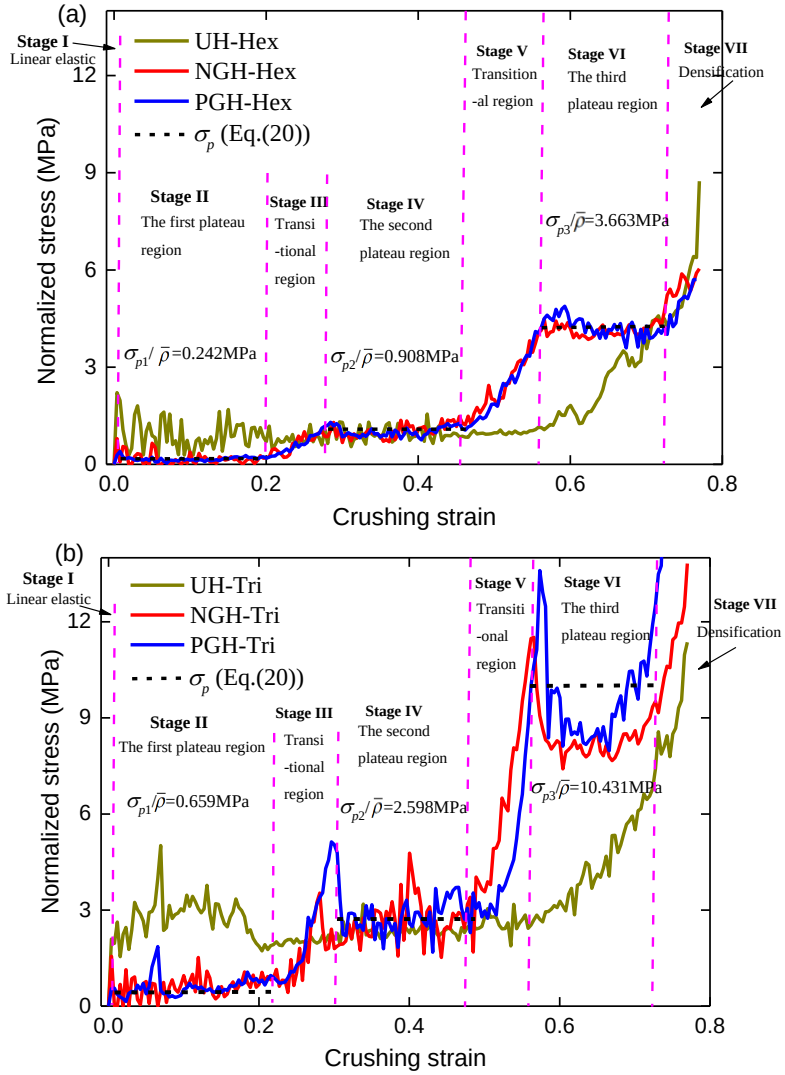

Fig. 13. In-plane crushing stress-strain relation of graded hierarchical honeycomb with (a) hexagonal and (b) triangular sub-structures under same conditions of Figs. 11 and 12. Seven stages including linear elastic and densification stages, as well as three plateau stages and two transitional stages can be identified.

4.2. Theoretical analysis of plateau stress

In this subsection, the plateau stress of the graded hierarchical honeycomb under in-plane dynamic crushing load is analyzed theoretically by using the two-scale method proposed by Qian and Chen [73]. The sub-structure sides of the graded hierarchical honeycomb are homogenized as continuous solid material yielding the perfectly plastic behavior. Based on the deformation modes predicted by FE simulation shown in Fig. 14(a), a simplified model with the basic deformation unit marked by a blue window is presented, as depicted in Fig. 14(b). During the deformation, the

inclined edges (red marked lines) are not only rotating about the vertex (Point O in Fig. 14(b)) toward the horizontal but also shortened due to compression. The rotation angle of the inclined edge OA can be calculated as $\Delta\theta = \pi/3$, and point A would move to point A' after densification. Hence, the dissipated energy involves the rotation of two plastic hinges (at Points O and A) and the shortened deformation of OA with a length of $\Delta L = |OA - OA'|$. It should be pointed out that the present theoretical model is just a simplified model that neglects the Poisson's ratio of the graded hierarchical honeycomb, and have neglected the plastic hinges appearing in the horizontal wall, which is only suitable to the graded hierarchical honeycomb with low-density hierarchical sub-cells.

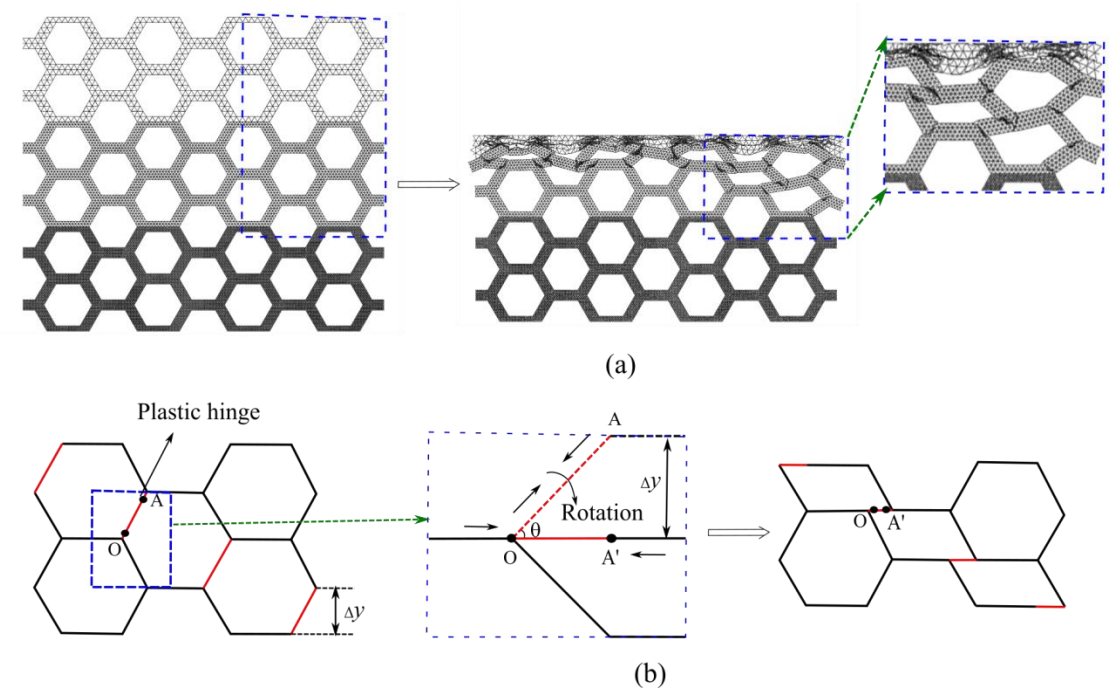

Fig. 14. Deformation mechanism for graded hierarchical honeycomb: (a) deformation pattern predicted by FE simulation; (b) simplified model for theoretical analysis.

Due to the symmetry of unit cell (marked by the blue window of Fig. 14(b)) about the central horizontal axis, only the top half model is taken into account, and the external work imposed on this half unit can be calculated as

$$W_{ex} = \frac{3}{2} N_i l_i b \sigma_{pi} \Delta y \,, \tag{13}$$

in which σ_{pi} is the plateau stress in i-th gradient layer of graded hierarchical honeycombs and $\Delta y = \sqrt{3} N_i l_i / 2$ denotes the moving displacement of the half unit when the inclined edge OA is horizontally deformed.

Based on the assumption of a perfectly plastic model for the homogenized sub-structure side, the bending moment generated by the plastic hinge can be expressed as

$$M_P = 2\int_0^{h/2} \sigma_p^{sub} by \mathrm{d}y = \frac{1}{4} bh^2 \sigma_p^{sub}, \tag{14}$$

in which σ_p^{sub} denotes the yield stress of the homogenized sub-structure side, and b is the out-of-plane depth of the honeycomb.

As the sub-structure side is made of triangular and hexagonal cellular structures, its equilateral yield stress σ_p^{sub} can be approximated by

$$\sigma_p^{sub} = C_{sub} \bar{\rho}_{sub}^2 \sigma_s, \tag{15}$$

where σ_s is the yield stress of the base material. The coefficient C_{sub} reflects the relationship between the equilateral yield stress (In-plane) and the relative density for the pure triangular or hexagonal honeycombs. The coefficient can be obtained by repeated simulations of the equilateral yield stress (In-plane) of pure triangular and hexagonal honeycombs with different relative densities, and obtain their relationship through the curve fitting procedure. During the simulation process, the BCs may also affect the predicted equilateral yield stress. To eliminate the influence of BCs, the out-of-plane deformation BCs of the established simulation model should be constrained to ensure the in-plane deformation condition. Additionally, a pure triangular and hexagonal honeycomb model with enough cell numbers should be established to eliminate the influence of surrounding edges.

In fact, this topic has been analyzed by several researchers, such as Gibson and Ashby [74] who systematically revealed the mechanical behaviors of honeycombs with different cell topologies. Qiao and Chen [73] analyzed the equilateral yield stress of pure triangular honeycombs, while the equilateral yield stress of pure hexagonal honeycombs was revealed by Qiu et al. [75]. Their studies all indicated that the equilateral yield stress is proportional to the second-order of the relative density of pure triangular and hexagonal honeycombs. Hence, C_{tri} = 0.534 [73] and C_{hex} = 0.271 [75] that are derived by previous studies are employed for triangular and hexagonal sub-structures, respectively.

Additionally, $\bar{\rho}_{sub}$ is the relative density of sub-structures, which can be separately denoted as

$$\begin{aligned} \bar{\rho}_{tri} &= \frac{6t}{\sqrt{3}l_i}, \qquad \text{Triangular sub-structure} \\ \bar{\rho}_{hex} &= \frac{2t}{\sqrt{3}l_i}, \qquad \text{Hexagonal sub-structure} \end{aligned} \tag{16}$$

The energy dissipated by the bending moment of the two plastic hinges can be denoted as

$$W_m = 2M_P \Delta\theta = \frac{\pi}{6} bh^2 \sigma_p^{sub}. \tag{17}$$

Apart from the energy dissipation of plastic hinges, the energy dissipated by the shortening deformation of OA is also to be taken into account. The shorten deformation of the inclined edge OA can be calculated as $\Delta L = |OA - OA'| = N_i l_i (1 - \cos\theta) = N_i l_i / 2$, and the cross-sectional area of this edge is $A = bh$. Hence, the plastic dissipation W_s can be derived as

$$W_s = A\sigma_p^{sub} \Delta L = \frac{1}{2} N_i l_i hb \sigma_p^{sub}. \tag{18}$$

The conservation of energy under the whole deformation process yields

$$W_{ex} = W_m + W_s. \tag{19}$$

By substituting Eqs. (13) - (18) into Eq. (19), leads to the plateau stress σ_{pi} as follows

$$\sigma_{pi} = \left[\frac{2\pi}{9\sqrt{3}} \frac{h^2}{\left(N_i l_i\right)^2} + \frac{2}{3\sqrt{3}} \frac{h}{N_i l_i} \right] \sigma_p^{sub}. \tag{20}$$

The collapse stresses predicted by the FE simulation and theoretical methods are compared in Fig. 13 for NGH-Tri and NGH-Hex honeycomb using dashed lines. It is evident that three plateau stages can be observed for the graded hierarchical honeycombs subjected to crushing loads, and the theoretical predictions agree well with the FE results for the plateau stress in all three plateau stages.

4.3. Graded hierarchical honeycombs with varying thickness

In this subsection, the low-velocity impact response of graded hierarchical honeycombs with varying thickness in each gradient layer is analyzed to give a comparison with that presented in Section 4.1. Herein, the impact velocity is specified as v = 3m/s, and the thickness of uniform hierarchical honeycombs is set as t = 0.05mm. To ensure the equivalent total mass between uniform and graded hierarchical honeycombs, $t_1 = 0.0935\text{mm}$, $t_2 = 0.05\text{mm}$, and $t_3 = 0.0259\text{mm}$ are employed for NGH-Tri honeycomb, and $t_1' = 0.0938\text{mm}$, $t_2' = 0.05\text{mm}$, and $t_3' = 0.0263\text{mm}$ are employed for NGH-Hex honeycomb. The deformation process of those graded hierarchical honeycombs with varying thickness is similar to these with uniform thickness presented in Figs.

11 and 12. Five stages including linear elastic and densification stages, as well as three plateau stages appear for this type of graded hierarchical honeycombs, as shown in Fig. 15. A slight difference for the plateau stress among different plateau stages can be observed, which is caused by the different topologies among different gradient layers. However, the plateau stress in all three plateau stages is slightly closer to the plateau stress of uniform hierarchical honeycombs, which is consistent with that predicted by the theoretical analysis. This is due to the fact that the total mass in each gradient layer are the same as that in the uniform hierarchical honeycomb.

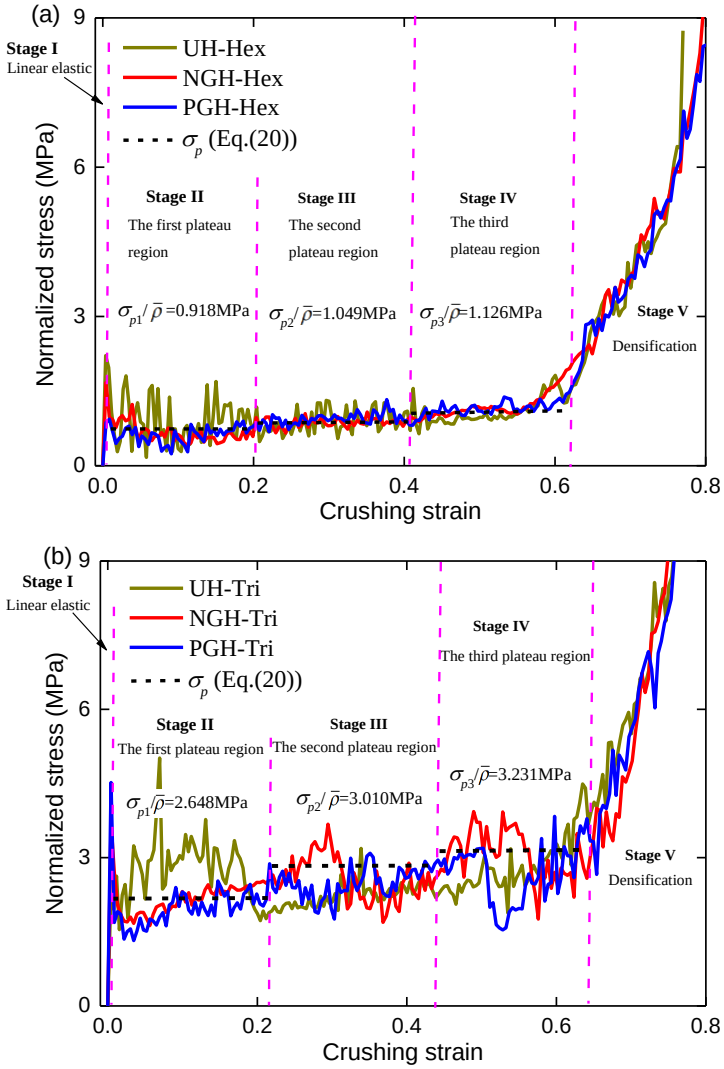

Fig. 15. In-plane crushing stress-strain relation of graded hierarchical honeycomb with (a) hexagonal and (b) triangular sub-structures, as well as with varying thickness in different gradient layers under impact velocity v = 3m/s. Five stages including linear elastic and densification stages, and three plateau stages are exhibited.

5. Parametric studies

Parametric studies are performed and presented in this section to investigate the effects of impact velocity, topology of sub-structures, gradient configuration, and wall thickness on the

deformation pattern and energy absorption of graded hierarchical honeycombs under crushing loadings. Three impact velocities including low, medium and high velocities are taken into account. Under experimental conditions, the low impact velocity can be obtained by using drop hammer, in which the strain rate is in the range of $0.1\sim10^3\ s^{-1}$. The medium speed with the strain rate $10^2\sim10^4\ s^{-1}$ can be achieved by the SHPB (Split Hopkinson Pressure Bar), while much higher impact velocity with the strain rate $10^3\sim10^5\ s^{-1}$ can be achieved by Taylor impact test [76]. The graded hierarchical honeycomb with uniform thickness is employed in the following studies if no otherwise specified.

5.1. High-velocity impact performance

As a comparison to the low-velocity deformation mode presented in Section 3.1, the high-velocity deformation patterns of graded hierarchical honeycombs under v = 60m/s are investigated in Figs. 16 and 17. As can be seen, the deformation pattern under high-velocity impact is greatly different from that under low-velocity impact. “I” deformation mode can be observed for both the uniform and graded hierarchical honeycombs under the high-velocity impact, i.e., the crushing deformation appears firstly in the impact end, and it will deform progressively to the supported end of the honeycomb. A clear shock front can be found for all honeycombs, i.e., the honeycomb is wholly crushed behind this front, while being almost un-deformed ahead of the front. The honeycomb in the support end is un-deformed during the whole crushing process until the shock front propagates to this end for all honeycombs, which is largely different from the low-velocity impact cases presented in Figs. 11 and 12.

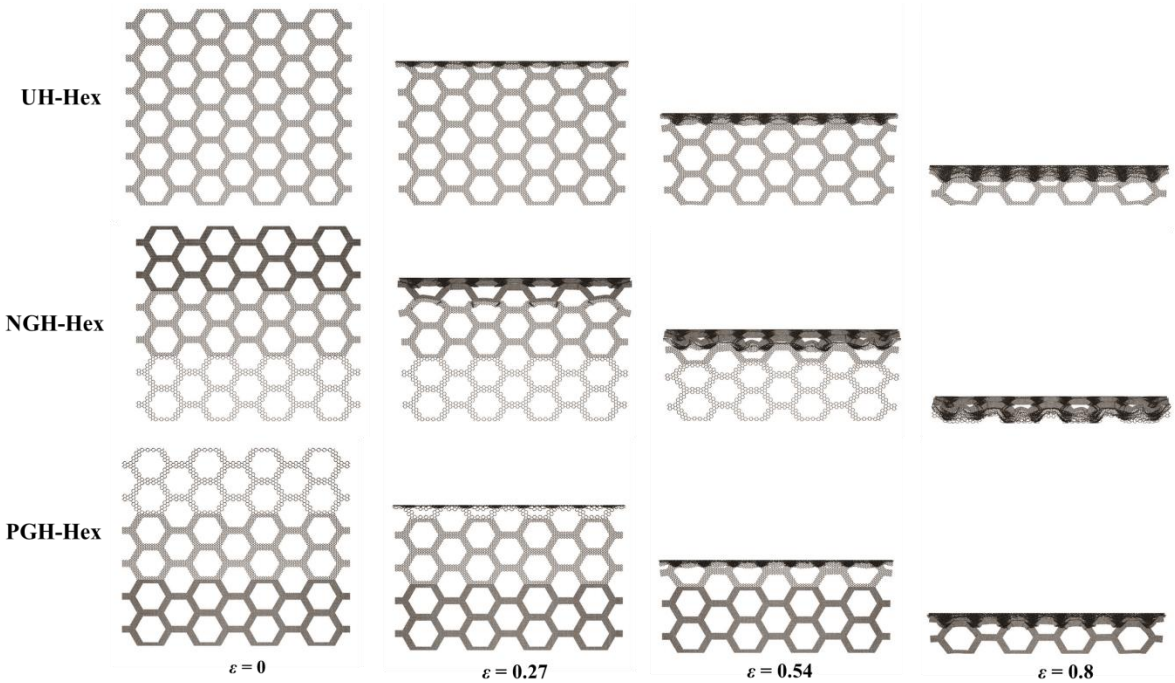

Fig. 16. Deformation pattern for graded hierarchical honeycombs with hexagonal sub-structures under high impact velocity v = 60m/s. "I" deformation mode is observed for all honeycombs.

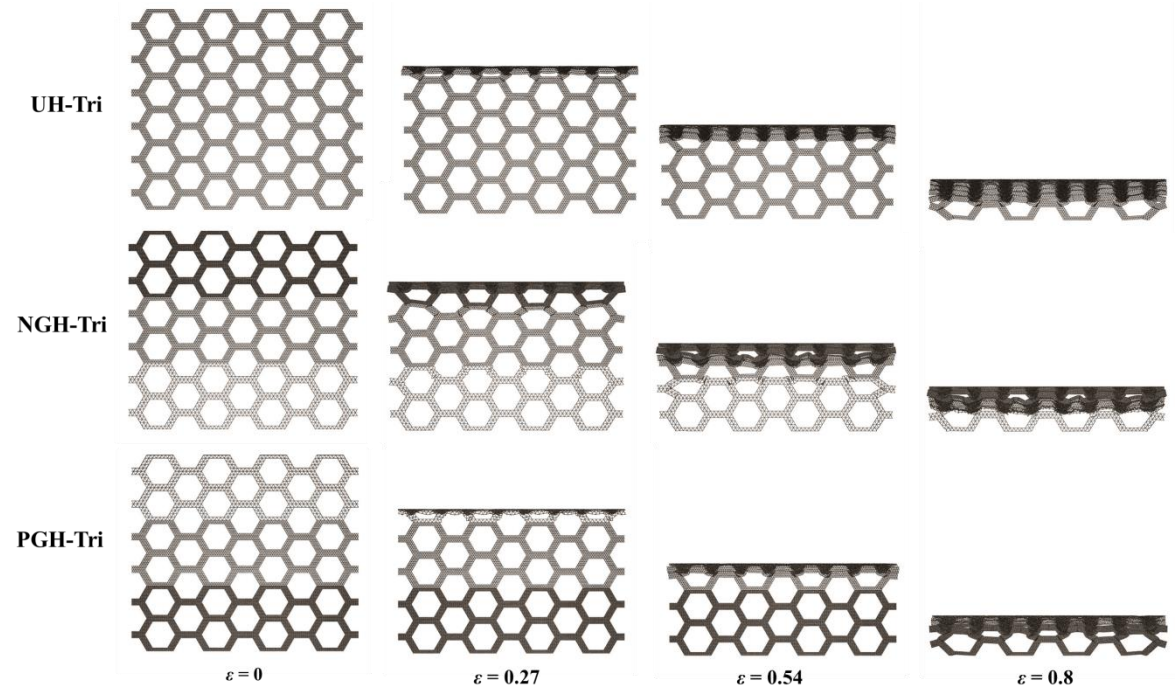

Fig. 17. Deformation pattern for graded hierarchical honeycombs with triangular sub-structures under high impact velocity v = 60m/s. "I" deformation mode is observed for all honeycombs.

For honeycomb-type structures under high-velocity impact, a typical characteristic is that lateral inertia will affect the dynamic stress greatly. The progressive "I" deformation mode can be observed due to the hardening phenomenon of cellular material, which can be physically explained by the shock wave theory [12, 46, 73]. Accordingly, the dynamic crushing stress under

high-velocity impact can be approximated by

$$\sigma_{di} = \sigma_{pi} + \frac{\rho_s \bar{\rho}_i}{\varepsilon_{di}} v^2 \tag{21}$$

in which σ_{pi} and σ_{di} represent the static and dynamic plateau stresses in i-th gradient layer of the graded hierarchical honeycomb, respectively. v and ρ_s are, respectively, the crushing velocity and density of the base material, and $\bar{\rho}_i$ denotes the relative density in i-th gradient layer of graded hierarchical honeycomb. Moreover, ε_{di} is the densification strain for i-th gradient layer of graded hierarchical honeycomb, which can be calculated as $\varepsilon_{di} = 0.8(1-\bar{\rho}_i)$ [73].

The high-velocity dynamic stress-strain curves of graded hierarchical honeycomb with hexagonal and triangular sub-structures are presented in Figs. 18(a) and (b), respectively. A significant difference to the low-velocity impact case (shown in Fig. 13) is that only five stages are exhibited in the high-velocity impact. Apart from the linear elastic and densification stages, one can also observe three plateau regions, while the transitional stages between two continuous plateau regions shown in Fig. 13 are vanished due to the effect of lateral inertia under high-velocity impact. Additionally, the dynamic stress of NGH and PGH honeycombs is different in the first plateau region because the relative density for their first crushed region is different, i.e., the first crushing region appears in the strong end of NGH and in the weak end of PGH, as shown on Figs. 16 and 17, which will lead to the stress $\sigma_{d1\_NGH} > \sigma_{d1\_PGH}$. A similar phenomenon is also observed in the third plateau region, in which the final crushing region appears in the weak end of NGH and in the strong end of PGH, leading to the stress $\sigma_{d3\_PGH} > \sigma_{d3\_NGH}$. The dynamic stress in Gradient layer 1 of NGH honeycomb is equal to that in Gradient layer 3 of PGH honeycomb due to the same relative density, i.e., $\sigma_{d1\_NGH} = \sigma_{d3\_PGH}$, meanwhile $\sigma_{d1\_PGH} = \sigma_{d3\_NGH}$ and $\sigma_{d2\_NGH} = \sigma_{d2\_PGH}$ also can be derived in a similar way. The dynamic stress predicted by the numerical method is verified well with that calculated by Eq. (21).

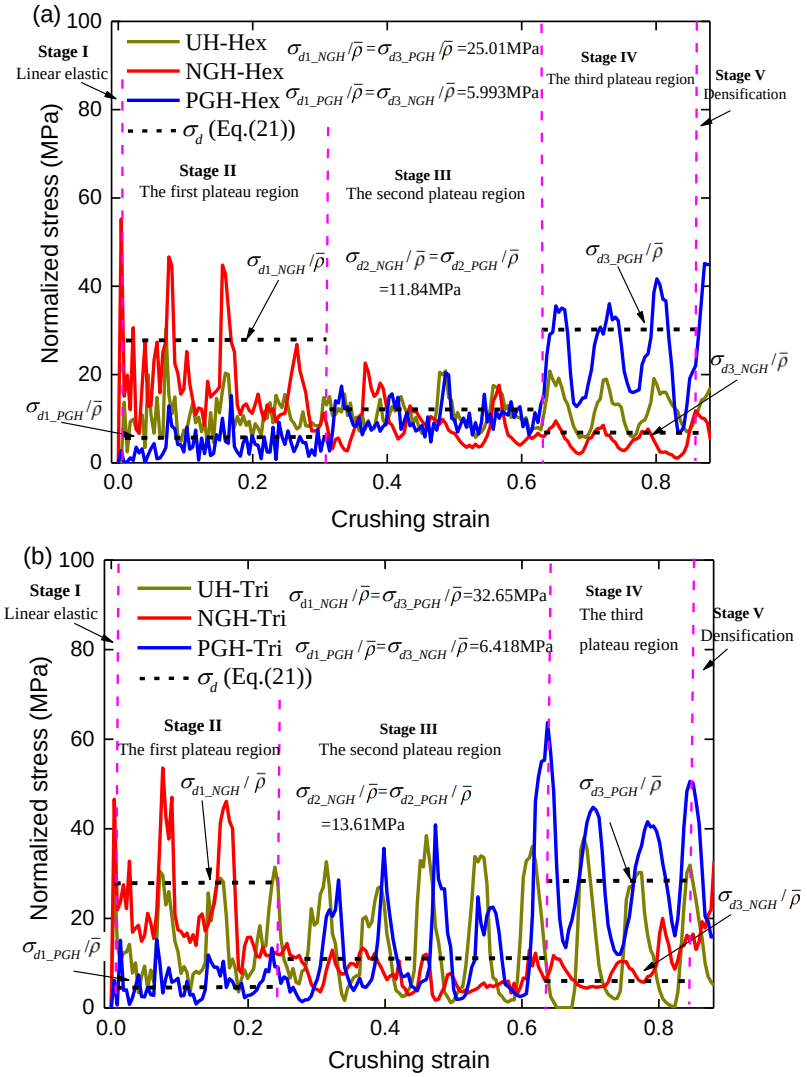

Fig. 18. In-plane crushing stress-strain relation of graded hierarchical honeycomb with (a) hexagonal and (b) triangular sub-structures under same conditions of Figs. 16 and 17. Five stages including linear elastic and densification stages, and three plateau stages are exhibited.

5.2. Effect of impact velocity

In this subsection, the influence of impact velocity on the in-plane crushing performance will be investigated. Firstly, the crushing stress-strain curves for NGH-Tri and PGH-Tri honeycombs under different impact velocities are examined in Fig. 19. It is evident that the crushing stress is enhanced as the impact velocity increases for all graded hierarchical honeycombs, which is attributed by the fact that the lateral inertia of cellular materials increases with impact velocity. The oscillation of stress can be observed in all stages of PGH-Tri honeycomb under impact velocities 40 and 60m/s, while it only appears in the first stage of NGH-Tri honeycomb. This phenomenon is attributed to the fact that the crushing proceeds gradually from weak to strong ends for PGH-Tri honeycomb, leading to oscillation of stress in each stage, and this oscillation is

much more significant under the crushing of strong region. For NGH-Tri honeycomb, the strong region will be crushed first under impact velocities of 40 and 60m/s, which will lead to significant oscillations in the first stage, and the crushed material during this stage can reduce the oscillation in the following stages. Additionally, three plateau stages are observed for all impact velocities, and the stress for each plateau stage is increased by increasing the impact velocity. For NGH-Tri honeycomb, the largest plateau stress occurs in the third plateau stage under low-velocity impact, while it transforms to the first plateau stage when the impact velocity becomes larger. This phenomenon can be explained by the fact that the first deformed region for NGH-Tri honeycomb is different under different impact velocities. In contrast, the largest plateau stress for PGH-Tri honeycomb always appears in the third plateau stage under all impact velocities.

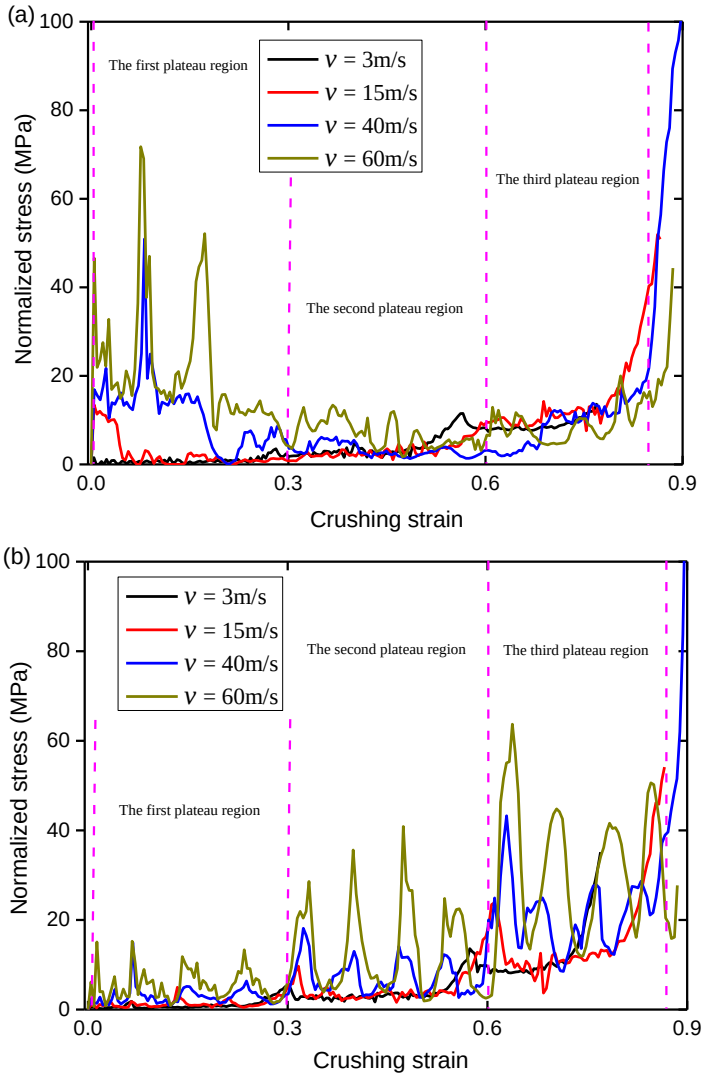

Fig. 19. In-plane crushing stress-strain relation for (a) NGH-Tri and (b) PGH-Tri honeycombs under different impact velocities. For PGH-Tri honeycomb, the largest plateau stress always appears in the third plateau stage, while it occurs in the third/ first plateau stage under low- /high- velocity impact for NGH-Tri honeycomb.

To further illustrate the influence of impact velocity on the crushing stress of the graded hierarchical honeycombs, the average crushing stress as a function of the impact velocity is presented in Fig. 20. Here, the NGH honeycombs with hexagonal and triangular sub-structures are taken into account, which gives a comparison with their uniform counterparts. The FE prediction of average crushing stress is calculated over the region before the densification stage via Eq. (11), while the theoretical prediction of this stress is obtained by calculating the average value of the three plateau stresses, i.e., $\sigma_{ave}= (\sigma_{d1}+\sigma_{d2}+\sigma_{d2})/3$ because the duration for each plateau stage is almost equivalent. One can find that the average crushing stress increases with the increment of impact velocity, which would lead to larger energy absorption. The average crushing stress of graded hierarchical honeycombs is larger than that of uniform hierarchical honeycombs, indicating that the graded hierarchical honeycomb can provide larger energy absorption capacities. Observably, the average crushing stress predicted by the theoretical analysis validates well with that obtained by the numerical method.

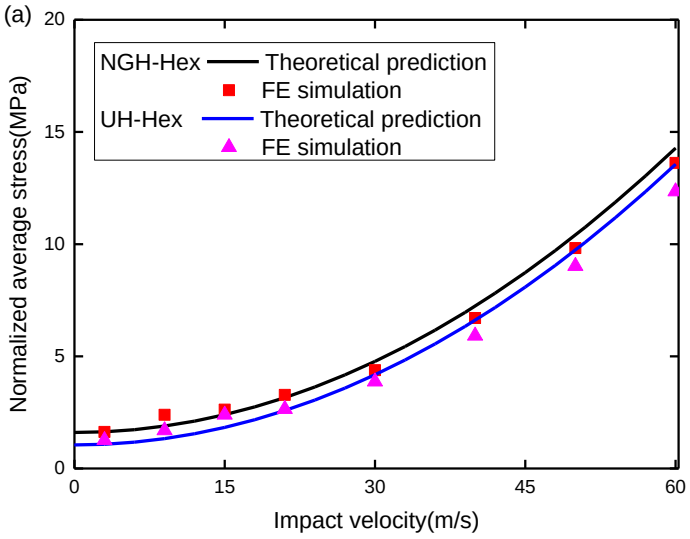

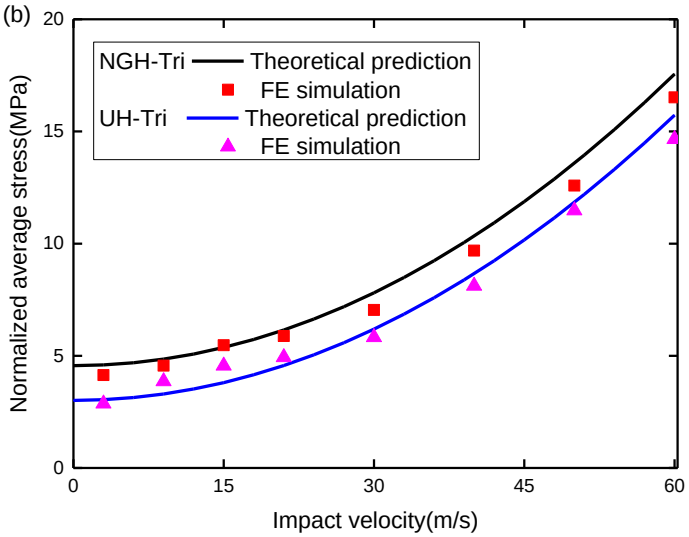

Fig. 20. Effect of impact velocity on average plateau stress of graded hierarchical honeycomb with (a) hexagonal and (b) triangular sub-structures. The average crushing stress increases as the impact velocity is enhanced for all honeycombs.

5.3. Energy absorption performance

The energy absorption behaviors of graded hierarchical honeycombs are examined in this subsection. As depicted in Figs. 21 and 22, the SEA versus strain curve for graded hierarchical honeycombs under low- and high-velocity impacts is compared. The crushing velocities v = 3 and 60 m/s are employed in Figs. 21 and 22 to represent the low- and high-velocity impacts, respectively. The SEA curves for NGH and PGH honeycombs are overlapped when the impact velocity is low, while exhibiting distinctions between them when the impact velocity becomes large.

From Fig. 21, the SEA of graded hierarchical honeycombs is slightly lower than that of uniform hierarchical honeycombs at small compression strains, but exceeds its uniform counterpart when the compression strain is larger than 0.6 under low-velocity impact. From Fig. 22, NGH honeycomb presents largest SEA while PGH honeycomb presents smallest SEA at small crushing strains, which is caused by the fact that the strongest and weakest regions are crushed first for NGH and PGH honeycombs, respectively, under high-velocity impact as depicted in Figs. 15 and 16. While a reversed behavior takes a place at large crushing strains, and the final crushed region are different for NGH and PGH honeycombs. Additionally, Fig. 22 also shows that the SEA of PGH honeycombs is always smaller than the UH honeycombs until the densification strain is achieved, indicating that positive gradient distribution can weaken the energy absorption performance of hierarchical honeycombs before the densification strain.

Focusing on NGH honeycombs, one can find that the NGH-Hex honeycomb can always present a larger SEA than UH-Hex honeycomb, while the SEA of NGH-Tri honeycomb is larger than UH-Tri honeycomb as $\varepsilon < 0.6$ and it becomes smaller than UH honeycomb when the strain exceeds 0.6. This physical phenomenon suggests the sub-structural configuration will significantly affect the SEA performance of graded hierarchical honeycombs.

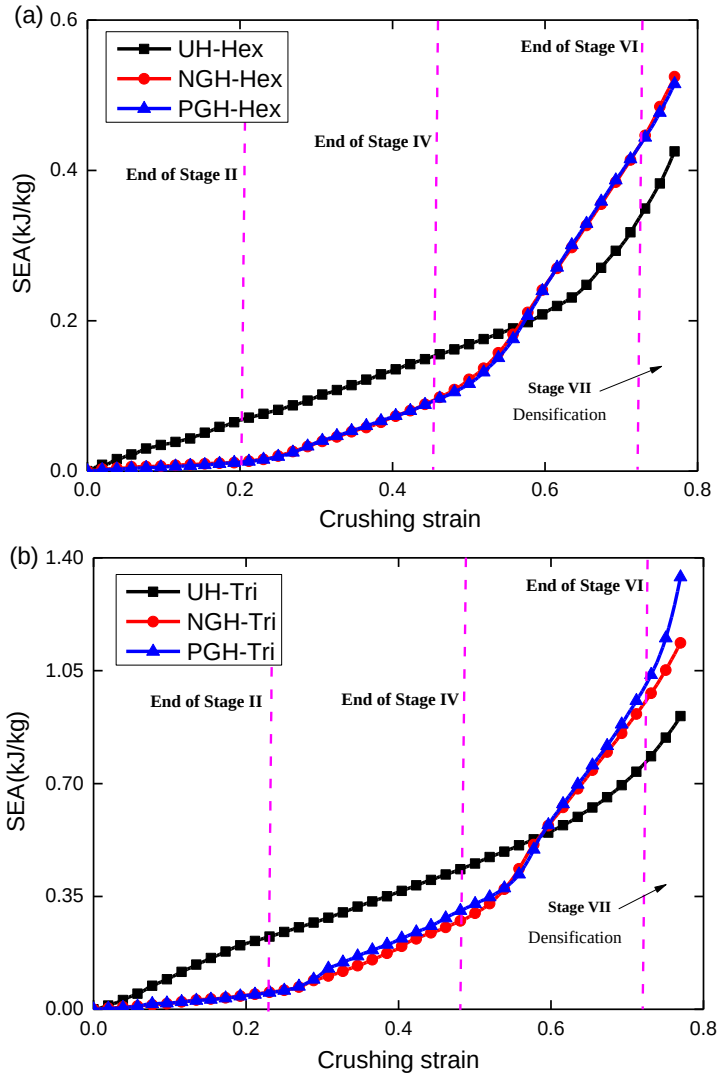

Fig. 21. SEA versus strain for graded hierarchical honeycombs with (a) hexagonal and (b) triangular sub-structures under low-velocity impact. The SEA curves for NGH and PGH honeycombs are almost overlapped.

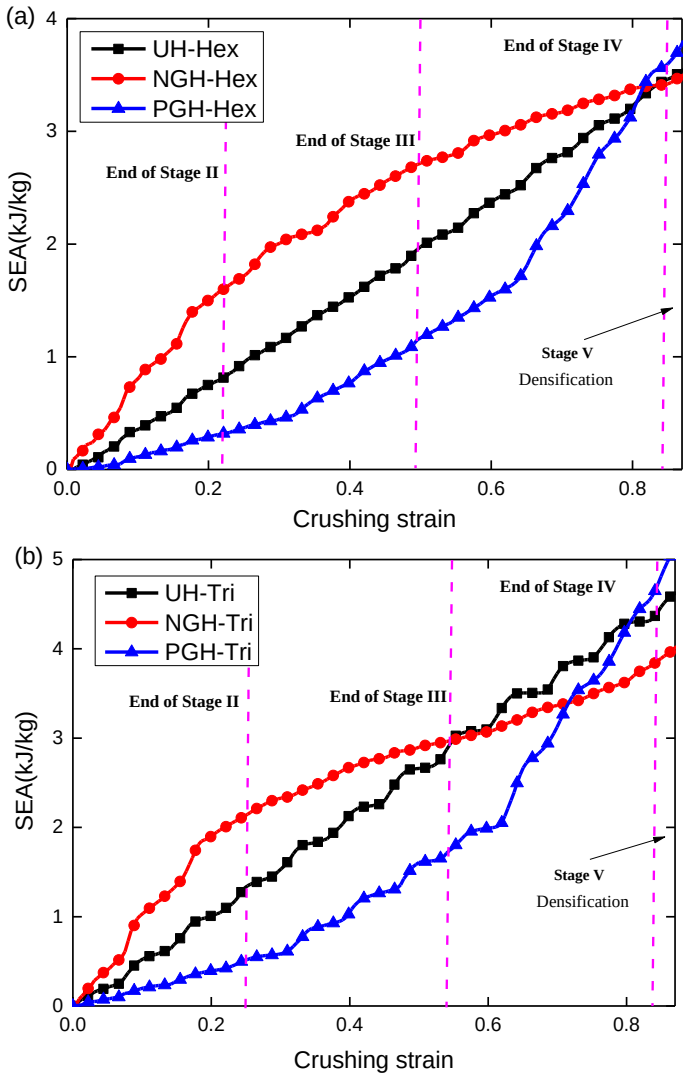

Fig. 22. SEA versus strain for graded hierarchical honeycombs with (a) hexagonal and (b) triangular sub-structures under high-velocity impact. The NGH honeycombs exhibit better SEA performance as compared to UH honeycombs at low strain, while PGH honeycombs perform better at densification strain.

The crushing behavior of uniform hierarchical honeycombs with hexagonal and triangular sub-structures has been analyzed by several different authors, including Chen et al. [45] who studied the crushing behavior of the UH-Tri honeycombs, Li et al. [46] who discussed the in-plane compression performance of UH-Hex honeycombs, and Yin et al. [47] who simultaneously analyzed the crushing behaviors of UH-Tri and UH-Hex honeycombs. To further explain the advantage of graded hierarchical honeycombs over the uniform hierarchical honeycombs, the SEA of graded hierarchical honeycombs at the densification strain is compared for different gradient and sub-structural configurations in Fig. 23. As observed, under low-velocity impact of v = 3m/s, the SEA for graded hierarchical honeycombs with hexagonal and triangular sub-structures is enhanced by 27.9% and 32.2%, respectively, as compared to their uniform counterparts. This

phenomenon suggests that the graded hierarchical design can present better energy absorption behaviors than the uniform hierarchical honeycombs introduced by previous studies [45-47]. Moreover, by comparing with the re-entrant hierarchical honeycombs conducted by Tan et al. [49], the proposed graded hierarchical honeycombs can deliver twice the amount of SEA.

As the impact velocity increases, the total absorbed energy by the graded hierarchical honeycombs is enhanced due to the lateral inertia effect, while SEA enhancement for graded hierarchical honeycombs to their uniform counterparts is reduced. Under high-velocity impact v = 60m/s, NGH-Hex honeycomb only provides 4.04% enhancement on the SEA as compared to the UH-Hex honeycomb, while the SEA of NGH-Tri honeycomb is only 5.25% larger than the uniform counterpart. Additionally, from Fig. 23(a), the graded hierarchical honeycomb with triangular sub-structures has better SEA performance than that with hexagonal sub-structures, and the SEA of NGH and PGH honeycombs with triangular sub-structures is almost 2.5 times larger than those with hexagonal sub-structures.

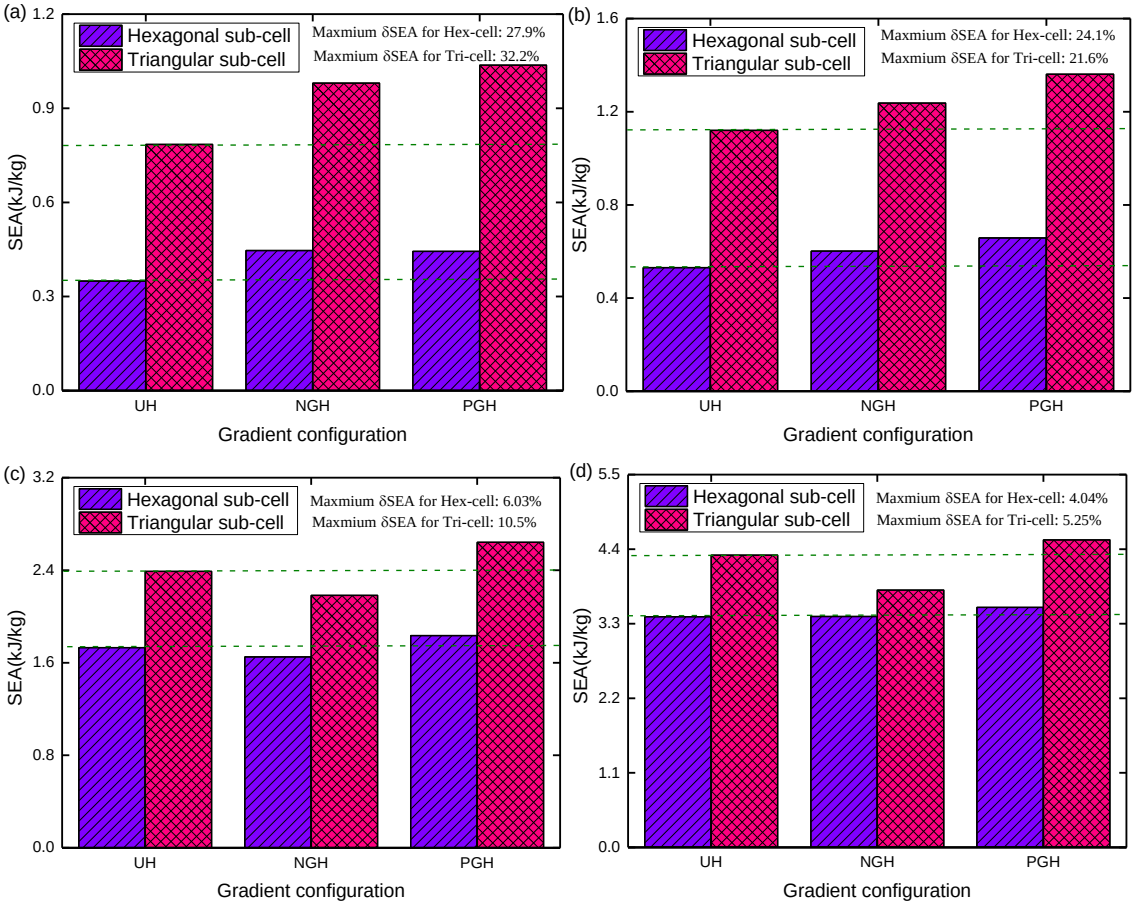

Fig. 23. SEA of graded hierarchical honeycombs under different impact velocities: (a) v = 3m/s; (b) v =15m/s; (c) v = 40m/s; (d) v = 60m/s. As the impact velocity increases, the SEA is enhanced for all graded hierarchical honeycombs, while the SEA enhancement for graded hierarchical honeycombs to their uniform counterparts is

reduced.

5.4. Effect of cell wall thickness

The wall thickness also plays an important role in the crushing stress and energy absorption performances of graded hierarchical honeycombs, which are explained in Figs. 24 and 25, respectively. Here, the impact velocity is specified as 21m/s, and three different cell thicknesses t = 0.05, 0.10, and 0.15mm are taken into account. Fig. 24 illustrates that the wall thickness can enhance the crushing stress for all graded hierarchical distributions, which is due to the fact that the relative density of the graded hierarchical is increased by increasing the wall thickness. For PGH-Tri honeycomb, one can find three plateau stages for all wall thicknesses. For NGH-Tri honeycomb, the third plateau region can be observed when the cell thickness t = 0.05mm, while it becomes unclear as the cell thickness is larger than 0.1mm. In the second plateau region, the stress-strain curve for the honeycomb with large cell thickness exhibits almost the same changing trend but enhanced magnitude as that with small cell thickness.

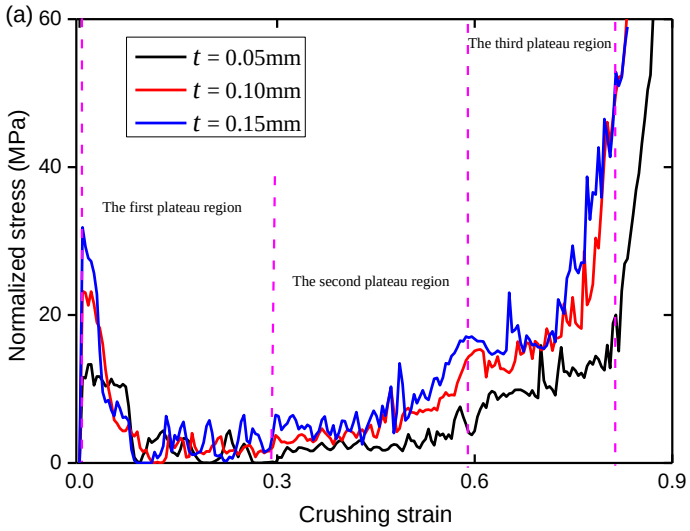

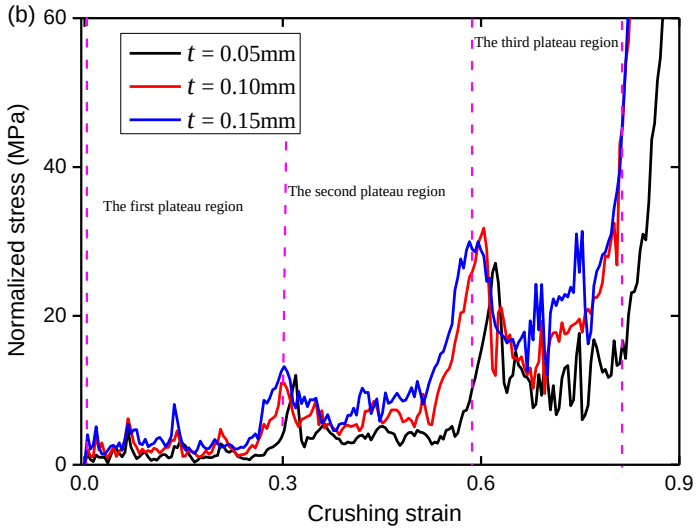

Fig. 24. In-plane crushing stress-strain relation for (a) NGH-Tri and (b) PGH-Tri honeycombs with different wall thicknesses. The crushing stress is increased by increasing the wall thickness for all graded hierarchical distributions.

The influence of wall thickness on SEA performance of graded hierarchical honeycombs is presented in Fig. 25 for hexagonal and triangular sub-structures. As observed, the SEA is enhanced for all graded hierarchical honeycombs by increasing the wall thickness. Almost all graded hierarchical configurations can perform better in SEA than the UH honeycomb, which is consistent with that shown in Fig. 23(b) under medium velocity impact. The maximum SEA enhancement over UH honeycombs for graded hierarchical honeycombs with triangular sub-structures is up to 22.5%, and can even reach 26.9% with hexagonal sub-structures. Moreover, the positive gradient configuration can provide better SEA performance than the negative gradient configuration, and the triangular sub-structure can produce a much larger SEA than the hexagonal sub-structure under medium velocity impact.

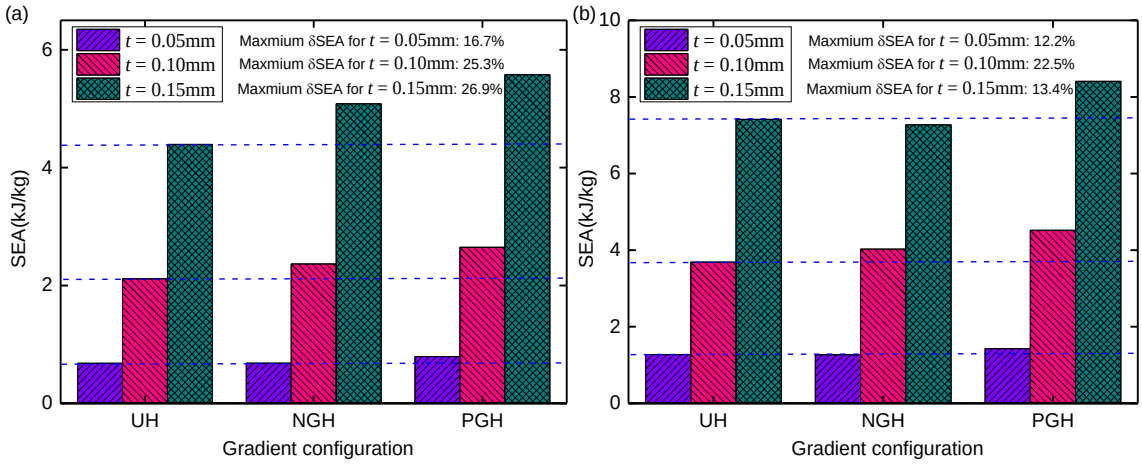

Fig. 25. Effect of wall thickness on SEA of graded hierarchical honeycombs with (a) hexagonal and (b) triangular

sub-structures. PGH honeycombs can provide better SEA performance than NGH honeycombs, and the triangular sub-cell can present a larger SEA than hexagonal sub-cell.

5.5. Result summarization

In this subsection, a summarization of the SEA and normalized average plateau stress ($\sigma_{ave}/\overline{\rho}$) is presented, as listed in Table 2. It is clear that the graded hierarchical honeycombs (NGH and PGH) can present higher energy absorption and crushing stress than the uniform hierarchical honeycombs (UH). Additionally, the graded hierarchical with triangular sub-cell (-Tri) can provide higher energy absorption and crushing stress than that with hexagonal sub-cell (-Hex). This comparison possesses the advantages of graded hierarchical design on enhancing the specific energy absorption capacities of honeycombs.

Table 2 Comparison for graded hierarchical honeycomb with different configurations.

Configuration	Hexagonal sub-cell (-Hex)			Triangular sub-cell(-Tri)		
	UH	NGH	PGH	UH	NGH	PGH
SEA(kJ/kg)	0.349	0.447	0.444	0.785	0.980	1.037
$\sigma_{ave}/\overline{\rho}$ (MPa)	1.284	1.647	1.657	2.886	3.596	3.839

6. Conclusion

In this work, a series of novel hexagonal honeycombs with graded hierarchical properties are presented to enhance their crashworthiness behaviors. The hierarchy is achieved by replacing cell walls of regular honeycombs with sub-structures and the gradient distribution can be obtained by varying the hierarchical length ratio in each layer. Both hexagonal and triangular configurations are employed as the sub-cell structures, and two gradient distributions including negative and positive graded hierarchies are compared. The crashworthiness and energy absorption behaviors of graded hierarchical honeycombs are numerically analyzed, which are also validated by comparing with previous experiments and theoretical predictions.

The deformation mode is highly dependent on the impact velocity, in which “I+V” deformation mode appears under low-velocity impact, while “I” deformation mode is observed under high-velocity impact. Seven stages including linear elastic and densification stages, as well as three plateau stages and two transitional stages, can be identified for the graded hierarchical honeycombs under low-velocity impact. However, the two transitional stages vanished when the

impact velocity is high, leading to a total of five stages in high-velocity impact. The crushing stress and SEA are both enhanced as the impact velocity enlarges due to the lateral inertia effect of cellular materials.

The gradient distribution will affect the crashworthiness performance of graded hierarchical honeycombs. The stress-strain and SEA-strain curves of NGH and PGH honeycombs are almost identical when the impact velocity is low, while a significant distribution can be observed as the impact velocity becomes high. Specifically, the largest plateau stress for NGH honeycomb occurs in the third plateau stage under the low-velocity impact, and it transforms to the first plateau stage under the high-velocity impact. However, the largest plateau stress for NGH honeycomb always appears in the third plateau stage under all impact velocities. Both the NGH and PGH distributions can enhance the SEA behavior under low-velocity impact, while only the PGH distribution can improve the SEA performance under high-velocity impact. Overall, the PGH configuration can provide better SEA performance than the NGH configuration

The sub-cell configuration also plays an important role on the crushing stress and energy absorption behaviors of graded hierarchical honeycombs. The triangular sub-structures possess better SEA than hexagonal sub-structures. The SEA enhancement for hexagonal and triangular sub-structures is up to 27.9% and 32.2%, respectively, as compared to their uniform counterparts under low-velocity impact. However, the hexagonal and triangular sub-structures only provide 4.04% and 5.25% SEA enhancement under high-velocity impact. The cell thickness can also enhance the crushing stress and energy absorption behaviors of graded hierarchical honeycombs.

Acknowledgments

The authors would like to thank the Singapore Centre for 3D Printing, which is supported by the National Research Foundation, Prime Minister’s Office, Singapore under its Medium-Sized Centre funding scheme, as well as the internal funding by Nanyang Technological University 04INS000329C160 and 04INS000453C160.

References

[1] Liu J, Chen W, Hao H, Wang Z. In-plane crushing behaviors of hexagonal honeycombs with different Poisson's ratio induced by topological diversity. Thin-Walled Structures 2021;159:107223.

[2] Li Z, Liu D, Qian Y, Wang Y, Wang T, Wang L. Enhanced strength and weakened dynamic sensitivity of honeycombs by parallel design. International Journal of Mechanical Sciences 2019;151:672-83.

[3] Ahmed N, Xue P. Governing the In-plane axial crushing of honeycomb with regular hexagonal

symmetric division cells using cross-hinge inserts. International Journal of Mechanical Sciences 2019;161-162:105062.
[4] Zhang X, Zhang H. Theoretical and numerical investigation on the crush resistance of rhombic and kagome honeycombs. Composite Structures 2013;96:143-52.
[5] Hu LL, Cai DY, Wu GP, He XL, Yu TX. Influence of internal pressure on the out-of-plane dynamic behavior of circular-celled honeycombs. International Journal of Impact Engineering 2017;104:64-74.
[6] Wang Z, Liu J. Numerical and theoretical analysis of honeycomb structure filled with circular aluminum tubes subjected to axial compression. Composites Part B: Engineering 2019;165:626-35.
[7] Sun D, Zhang W, Zhao Y, Li G, Xing Y, Gong G. In-plane crushing and energy absorption performance of multi-layer regularly arranged circular honeycombs. Composite Structures 2013;96:726-35.
[8] Gu H, Pavier M, Shterenlikht A. Experimental study of modulus, strength and toughness of 2D triangular lattices. International Journal of Solids and Structures 2018;152-153:207-16.
[9] Sun D, Zhang W. Energy absorption performance of staggered triangular honeycombs under in-plane crushing loadings. Journal of Engineering Mechanics 2013;139:153-66.
[10] Wang Z. Recent advances in novel metallic honeycomb structure. Composites Part B: Engineering 2019;166:731-41.
[11] Zhang Q, Yang X, Li P, Huang G, Feng S, Shen C, et al. Bioinspired engineering of honeycomb structure – Using nature to inspire human innovation. Progress in Materials Science 2015;74:332-400.
[12] Ruan D, Lu G, Wang B, Yu TX. In-plane dynamic crushing of honeycombs - A finite element study. International Journal of Impact Engineering 2003;28:161-82.
[13] Hu LL, Yu TX. Dynamic crushing strength of hexagonal honeycombs. International Journal of Impact Engineering 2010;37:467-74.
[14] Hu LL, Yu TX. Mechanical behavior of hexagonal honeycombs under low-velocity impact - Theory and simulations. International Journal of Solids and Structures 2013;50:3152-65.
[15] Wierzbicki T. Crushing analysis of metal honeycombs. International Journal of Impact Engineering 1983;1:157-74.
[16] Tao Y, Chen M, Chen H, Pei Y, Fang D. Strain rate effect on the out-of-plane dynamic compressive behavior of metallic honeycombs: Experiment and theory. Composite Structures 2015;132:644-51.
[17] Catapano A, Montemurro M. A multi-scale approach for the optimum design of sandwich plates with honeycomb core. Part I: homogenisation of core properties. Composite Structures 2014;118:664-76.
[18] Catapano A, Montemurro M. A multi-scale approach for the optimum design of sandwich plates with honeycomb core. Part II: the optimisation strategy. Composite Structures 2014;118:677-90.
[19] Montemurro M, Catapano A, Doroszewski D. A multi-scale approach for the simultaneous shape and material optimisation of sandwich panels with cellular core. Composites Part B: Engineering 2016;91:458-72.
[20] He Q, Feng J, Zhou H. A numerical study on the in-plane dynamic crushing of self-similar hierarchical honeycombs. Mechanics of Materials 2019;138:103151.
[21] Liang H, Wang Q, Pu Y, Zhao Y, Ma F. In-plane compressive behavior of a novel self-similar hierarchical honeycomb with design-oriented crashworthiness. International Journal of Mechanical Sciences 2021:106723.
[22] Shen L, Wang Z, Wang X, Wei K. Negative Poisson's ratio and effective Young's modulus of a vertex-based hierarchical re-entrant honeycomb structure. International Journal of Mechanical Sciences 2021;206:106611.

[23] Zhang Y, Lu M, Wang CH, Sun G, Li G. Out-of-plane crashworthiness of bio-inspired self-similar regular hierarchical honeycombs. Composite Structures 2016;144:1-13.
[24] Yang X, Sun Y, Yang J, Pan Q. Out-of-plane crashworthiness analysis of bio-inspired aluminum honeycomb patterned with horseshoe mesostructure. Thin-Walled Structures 2018;125:1-11.
[25] Zhang X-c, An C-c, Shen Z-f, Wu H-x, Yang W-g, Bai J-p. Dynamic crushing responses of bio-inspired re-entrant auxetic honeycombs under in-plane impact loading. Materials Today Communications 2020;23:100918.
[26] Yang X, Xi X, Pan Q, Liu H. In-plane dynamic crushing of a novel circular-celled honeycomb nested with petal-shaped mesostructure. Composite Structures 2019;226:111219.
[27] Li Z, Yang Q, Fang R, Chen W, Hao H. Crushing performances of Kirigami modified honeycomb structure in three axial directions. Thin-Walled Structures 2021;160:107365.
[28] Li Z, Yang Q, Fang R, Chen W, Hao H. Origami metamaterial with two-stage programmable compressive strength under quasi-static loading. International Journal of Mechanical Sciences 2021;189:105987.
[29] Bodaghi M, Liao WH. 4D printed tunable mechanical metamaterials with shape memory operations. Smart Materials and Structures 2019;28:045019.
[30] Bodaghi M, Serjouei A, Zolfagharian A, Fotouhi M, Rahman H, Durand D. Reversible energy absorbing meta-sandwiches by FDM 4D printing. International Journal of Mechanical Sciences 2020;173:105451.
[31] Zeng C, Liu L, Bian W, Leng J, Liu Y. Compression behavior and energy absorption of 3D printed continuous fiber reinforced composite honeycomb structures with shape memory effects. Additive Manufacturing 2021;38:101842.
[32] Bertolino G, Montemurro M, De Pasquale G. Multi-scale shape optimisation of lattice structures: an evolutionary-based approach. International Journal on Interactive Design and Manufacturing (IJIDeM) 2019;13:1565-78.
[33] Montemurro M, Bertolino G, Roiné T. A general multi-scale topology optimisation method for lightweight lattice structures obtained through additive manufacturing technology. Composite Structures 2021;258:113360.
[34] Ha NS, Pham TM, Hao H, Lu G. Energy absorption characteristics of bio-inspired hierarchical multi-cell square tubes under axial crushing. International Journal of Mechanical Sciences 2021;201:106464.
[35] Wang Z, Zhou Y, Wang X, Wei K. Compression behavior of strut-reinforced hierarchical lattice—Experiment and simulation. International Journal of Mechanical Sciences 2021;210:106749.
[36] Yang M, Han B, Su P, Zhang Q, Zhang Q, Zhao Z, et al. Crashworthiness of hierarchical truncated conical shells with corrugated cores. International Journal of Mechanical Sciences 2021;193:106171.
[37] Chen Y, Ma Y, Yin Q, Pan F, Cui C, Zhang Z, et al. Advances in mechanics of hierarchical composite materials. Composites Science and Technology 2021;214:108970.
[38] Ha NS, Lu G. A review of recent research on bio-inspired structures and materials for energy absorption applications. Composites Part B: Engineering 2020;181:107496.
[39] Reznikov N, Bilton M, Lari L, Stevens MM, Kröger R. Fractal-like hierarchical organization of bone begins at the nanoscale. Science 2018;360:aao2189.
[40] Habibi MK, Samaei AT, Gheshlaghi B, Lu J, Lu Y. Asymmetric flexural behavior from bamboo's functionally graded hierarchical structure: underlying mechanisms. Acta biomaterialia 2015;16:178-86.

[41] Zhan T, Sun F, Lyu C, He Q, Xu K, Zhang Y, et al. Moisture diffusion properties of graded hierarchical structure of bamboo: Longitudinal and radial variations. Construction and Building Materials 2020;259:119641.
[42] Sun Y, Wang B, Pugno N, Wang B, Ding Q. In-plane stiffness of the anisotropic multifunctional hierarchical honeycombs. Composite Structures 2015;131:616-24.
[43] Sun Y, Pugno NM. In plane stiffness of multifunctional hierarchical honeycombs with negative Poisson's ratio sub-structures. Composite Structures 2013;106:681-9.
[44] Chen Q, Pugno NM. In-plane elastic buckling of hierarchical honeycomb materials. European Journal of Mechanics - A/Solids 2012;34:120-9.
[45] Chen Y, Li T, Jia Z, Scarpa F, Yao C-W, Wang L. 3D printed hierarchical honeycombs with shape integrity under large compressive deformations. Materials & Design 2018;137:226-34.
[46] Li S, Liu Z, Shim VPW, Guo Y, Sun Z, Li X, et al. In-plane compression of 3D-printed self-similar hierarchical honeycombs – Static and dynamic analysis. Thin-Walled Structures 2020;157:106990.
[47] Yin H, Huang X, Scarpa F, Wen G, Chen Y, Zhang C. In-plane crashworthiness of bio-inspired hierarchical honeycombs. Composite Structures 2018;192:516-27.
[48] Huang W, Zhang Y, Xu Y, Xu X, Wang J. Out-of-plane mechanical design of bi-directional hierarchical honeycombs. Composites Part B: Engineering 2021;221:109012.
[49] Tan HL, He ZC, Li KX, Li E, Cheng AG, Xu B. In-plane crashworthiness of re-entrant hierarchical honeycombs with negative Poisson's ratio. Composite Structures 2019;229:111415.
[50] Dong L. Mechanical response of Ti–6Al–4V hierarchical architected metamaterials. Acta Materialia 2019;175:90-106.
[51] Yin S, Chen H, Li J, Yu TX, Xu J. Effects of architecture level on mechanical properties of hierarchical lattice materials. International Journal of Mechanical Sciences 2019.
[52] Zhang Xc, An Lq, Ding Hm. Dynamic crushing behavior and energy absorption of honeycombs with density gradient. Journal of Sandwich Structures and Materials 2014;16:125-47.
[53] Li Z, Jiang Y, Wang T, Wang L, Zhuang W, Liu D. In-plane crushing behaviors of piecewise linear graded honeycombs. Composite Structures 2019;207:425-37.
[54] Mousanezhad D, Ghosh R, Ajdari A, Hamouda AMS, Nayeb-Hashemi H, Vaziri A. Impact resistance and energy absorption of regular and functionally graded hexagonal honeycombs with cell wall material strain hardening. International Journal of Mechanical Sciences 2014;89:413-22.
[55] Shen CJ, Lu G, Yu TX. Dynamic behavior of graded honeycombs – A finite element study. Composite Structures 2013;98:282-93.
[56] Galehdari SA, Kadkhodayan M, Hadidi-Moud S. Low velocity impact and quasi-static in-plane loading on a graded honeycomb structure; experimental, analytical and numerical study. Aerosp Sci Technol 2015;47:425-33.
[57] Bates SRG, Farrow IR, Trask RS. Compressive behaviour of 3D printed thermoplastic polyurethane honeycombs with graded densities. Materials & Design 2019;162:130-42.
[58] Zhang J, Lu G, Ruan D, Huang X. Experimental observations of the double shock deformation mode in density graded honeycombs. International Journal of Impact Engineering 2019;134:103386.
[59] Xiao D, Dong Z, Li Y, Wu W, Fang D. Compression behavior of the graded metallic auxetic reentrant honeycomb: Experiment and finite element analysis. Materials Science and Engineering: A 2019;758:163-71.
[60] Nian Y, Wan S, Li X, Su Q, Li M. How does bio-inspired graded honeycomb filler affect energy absorption characteristics? Thin-Walled Structures 2019;144:106269.

[61] Li S, Li X, Wang Z, Wu G, Lu G, Zhao L. Sandwich panels with layered graded aluminum honeycomb cores under blast loading. Composite Structures 2017.
[62] Xiao L, Song W. Additively-manufactured functionally graded Ti-6Al-4V lattice structures with high strength under static and dynamic loading: Experiments. International Journal of Impact Engineering 2018;111:255-72.
[63] Mahbod M, Asgari M. Elastic and plastic characterization of a new developed additively manufactured functionally graded porous lattice structure: Analytical and numerical models. International Journal of Mechanical Sciences 2019;155:248-66.
[64] Al-Saedi DSJ, Masood SH, Faizan-Ur-Rab M, Alomarah A, Ponnusamy P. Mechanical properties and energy absorption capability of functionally graded F2BCC lattice fabricated by SLM. Materials & Design 2018;144:32-44.
[65] Al-Ketan O, Lee DW, Rowshan R, Abu Al-Rub RK. Functionally graded and multi-morphology sheet TPMS lattices: Design, manufacturing, and mechanical properties. J Mech Behav Biomed Mater 2020;102:103520.
[66] Li S, Hu M, Xiao L, Song W. Compressive properties and collapse behavior of additively-manufactured layered-hybrid lattice structures under static and dynamic loadings. Thin-Walled Structures 2020;157:107153.
[67] Montemurro M, Refai K, Catapano A. Thermal design of graded architected cellular materials through a CAD-compatible topology optimisation method. Composite Structures 2022;280:114862.
[68] Bai L, Gong C, Chen X, Sun Y, Xin L, Pu H, et al. Mechanical properties and energy absorption capabilities of functionally graded lattice structures: Experiments and simulations. International Journal of Mechanical Sciences 2020;182:105735.
[69] Liu H, Zhang ET, Ng BF. In-plane dynamic crushing of a novel honeycomb with functionally graded fractal self-similarity. Composite Structures 2021;270:114106.
[70] Rahman H, Yarali E, Zolfagharian A, Serjouei A, Bodaghi M. Energy Absorption and Mechanical Performance of Functionally Graded Soft-Hard Lattice Structures. Materials (Basel) 2021;14.
[71] Liu H, Chng ZXC, Wang G, Ng BF. Crashworthiness improvements of multi-cell thin-walled tubes through lattice structure enhancements. International Journal of Mechanical Sciences 2021;210:106731.
[72] Karagiozova D, Nurick GN, Chung Kim Yuen S. Energy absorption of aluminium alloy circular and square tubes under an axial explosive load. Thin-Walled Structures 2005;43:956-82.
[73] Qiao J, Chen C. In-plane crushing of a hierarchical honeycomb. International Journal of Solids and Structures 2016;85-86:57-66.
[74] Gibson LJ, Ashby MF. Cellular solids: structure and properties. Cambridge, UK: Cambridge university press; 1997.
[75] Qiu X, Zhang J, Yu T. Collapse of periodic planar lattices under uniaxial compression, part I: quasi-static strength predicted by limit analysis. International journal of impact engineering 2009;36:1223-30.
[76] Sun Y, Li QM. Dynamic compressive behaviour of cellular materials: a review of phenomenon, mechanism and modelling. International Journal of Impact Engineering 2018;112:74-115.